SPOROCYTELESS/NOZZLE acts together with MADS-domain transcription factors to regulate an auxin-dependent network controlling the Megaspore Mother Cell development

Alex Cavalleri[1,6], Chiara Astori[1,6], Silvia Manrique[1,3,6], Greta Bruzzaniti[1], Cezary Smaczniak[2], Chiara Mizzotti[1], Alessandro Ruiu[1], Mattia Spanò[1], Andrea Movilli[1,4], Veronica Gregis[1], Xiaocai Xu[2,5], Kerstin Kaufmann[2], Lucia Colombo[1,7]

[1]Departiment of Biosciences, University of Milan, Milano 20133, Italy.

[2] Plant Cell and Molecular Biology, Institute of Biology, Humboldt-Universität zu Berlin, Berlin 10115, Germany.

[3]Present address: Instituto de Biología Molecular y Celular de Plantas (IBMCP) (CSIC-UPV), Valencia, Spain / Departamento de Biología Vegetal, Facultad de Farmacia, Universidad de Valencia, Valencia, Spain.

[4]Present address: Department of Molecular Biology, Max Planck Institute for Biology Tübingen, 72076 Tübingen, Germany

[5]Present address: Department of physiology, Max Planck Institute for Biology Potsdam, 14476 Potsdam Brandenburg, Germany

[6]These authors contributed equally

[7]Correspondence to: lucia.colombo@unimi.it

Abstract

The formation of the female gamete is a complex developmental process that begins with the differentiation of the Megaspore Mother Cell (MMC) within the ovule.

SPOROCYTELESS/NOZZLE (SPL/NZZ) is the principal regulator of the MMC formation, as mutations in the *SPL/NZZ* gene lead to the failure of the MMC differentiation. Nonetheless, the SPL/NZZ-dependent regulatory pathway governing the MMC development remains largely unknown. Using a multi-omics approach, we identify direct SPL/NZZ targets and their downstream network. We discovered that SPL/NZZ interacts with ovule-identity MADS-domain transcription factor complexes, to regulate the expression of common target genes. By integrating the omics data with the analysis of either complementation or mutant lines, we describe a comprehensive regulatory mechanism, in which SPL/NZZ determines the differentiation of the MMC by acting on an auxin-dependent downstream network.

Introduction

In flowering plants, sporogenesis starts with the differentiation of female and male meiocytes: Megaspore Mother Cells (MMCs) within ovules and Pollen Mother Cells (PMCs) within anthers[1,2]. In *Arabidopsis thaliana,* the master regulator of meiocytes differentiation is *SPOROCYTELESS/NOZZLE (SPL/NZZ)* since mutations in the *SPL/NZZ* gene result in a complete female and male sterility due to the absence of both the MMC and the PMC[1,2]. *SPL/NZZ* belongs to the SPEAR family which, in *A. thaliana*, consists of 5 genes[3,4]. The SPEAR proteins have a nuclear localisation signal (NLS) at the N-terminus, the SPL/NZZ motif in the middle of the protein, and an EAR motif at the C-terminus. It has been reported that, through the EAR motif, SPL/NZZ recruits co-repressors, like TOPLESS (TPL), that mediate the transcriptional repression of target genes by interacting with HDAs[3–7].

SPL/NZZ also has an additional Myc-type helix-loop-helix domain that could mediate SPL/NZZ homodimerization[2,4]. Interestingly, SPL/NZZ was initially described as a MADS-like protein, since it contains a sequence of 17 amino acids similar to the MADS-domain[2].

According to earlier reports, SPL/NZZ can interact with two families of transcription factors (TFs): the YABBY (YAB) and the CINCINNATA-like TEOSINTE BRANCHED/CYCLOIDEA/PCF (TCP). SPL interaction with these TFs mediates the transcriptional repression of their targets in plants[4,5,8].

Despite its importance for plant reproduction, the mechanisms of *SPL/NZZ* transcriptional regulation, as well as its downstream network, are still poorly understood. Among the factors involved in *SPL/NZZ* regulation, auxin signalling was shown to be a positive regulator of *SPL/NZZ* expression in anthers, as demonstrated by the reduced *SPL/NZZ* transcript accumulation in the *taa1 tar2-2* mutant[9]. AGAMOUS (AG) is one of the few factors described to regulate *SPL/NZZ* expression in both ovules and stamens. Indeed, in flowers at stages 11-13[10], AG binds a CArG-box in the *SPL/NZZ* 3' UTR to promote its expression in integuments and chalaza of the ovule. Here, *SPL/NZZ* expression pattern is also regulated by the RdDM pathway, since *SPL/NZZ* is ectopically expressed in the *drm1drm2* mutant[11].

In addition to its function in MMC and PMC differentiation, SPL/NZZ is required for ovule patterning, by negatively regulating the expression of factors such as *AINTEGUMENTA (ANT)*, *BELL1 (BEL1)*, *INNER-NO-OUTER (INO)*, and *PHABULOSA (PHB)*[12,13]. Indeed, besides the absence of the MMC, *spl/nzz* mutant ovules are characterised by an impairment in integuments growth and a longer funiculus[12].

Concerning the SPL/NZZ downstream network, SPL/NZZ plays a crucial role in the auxin signalling pathway as the auxin-response reporter line *DR5v2* and the auxin efflux carrier *PIN-FORMED1 (PIN1)* exhibit decreased expression in the *spl/nzz* mutant ovule[14,15].

This study employs a multi-techniques approach, integrating Co-immunoprecipitation coupled with mass spectrometry (Co-IP/MS), Chromatin Immunoprecipitation and sequencing (ChIP-seq), and RNA sequencing (RNA-seq), to comprehensively identify direct SPL/NZZ targets and their downstream network. Our findings reveal the interaction between SPL/NZZ and ovule identity MADS-domain transcription factor complexes, thereby regulating the expression of common target genes, such as *ANT*. This activity influences the auxin signalling, which was previously suggested as a primary pathway necessary for the MMC differentiation[15]. We propose a multistep model in which MMC specification and development relies on an auxin-dependent SPL/NZZ downstream network.

Results

SPL/NZZ and MADS-domain transcription factors interact to form multimeric complexes

To gain insight into the network regulated by SPL/NZZ, essential for the specification of the MMC, we identified potential partners of SPL/NZZ during the early stages of ovule development, prior to and at the MMC stage, by performing co-immunoprecipitation followed by mass spectrometry (Co-IP/MS). To do this, we took advantage of the *pSPL/NZZ::SPL/NZZ:GFP* construct, previously used to complement the *spl-1* mutant allele[11].

As previously described[11], at ovule stage 2-I[16], SPL/NZZ-GFP accumulated in the most apical cells of the L1 layer (Supplementary Figure 1A). From stages 2-II to stage 2-V, associated with the end of the meiosis, SPL/NZZ-GFP accumulation domain comprised the L1 layer of the whole nucellus (Supplementary Figure 1B-D). At later stages, SPL/NZZ-GFP signal decreased without changing its pattern (Supplementary Figure 1E, F).

We introduced the *pSPL/NZZ::SPL/NZZ:GFP* construct into the *pAP1::AP1:GR ap1cal* system for synchronised induction of flower development[17,18]. We performed DEX treatment on the inflorescences and evaluated the SPL/NZZ-GFP expression at different days after induction (DAI) to select prior to and at the MMC stage for samples collection. At 3 DAI, SPL/NZZ-GFP was mainly visible in anther primordia, a result in line with SPL/NZZ activity in anther morphogenesis[2,19] (Supplementary Figure 1G-I). At 9 DAI, SPL/NZZ-GFP

expression in anthers was almost absent (Supplementary Figure 1J). By contrast, despite the partial loss of synchronisation at this later timepoint after AP1-GR induction, most flowers showed ovules at stage 2-I, where we could clearly observe a strong and specific nucellar SPL/NZZ-GFP accumulation (Supplementary Figure 1K-L).

Therefore, we used three independent biological replicates of inflorescences at 9 DAI for Co-IP/MS, employing an anti-GFP antibody[20]. We found 660 proteins that were statistically enriched ($\log_2$ intensity difference > 0; FDR ≤ 0.05) in the IP samples with respect to the input controls (Supplementary Data 1). As expected, SPL/NZZ itself was found as one of the most enriched proteins (Figure 1A; Supplementary Data 1).

To obtain an overview regarding the function of the protein enriched in the SPL/NZZ Co-IP/MS, we performed a molecular function and biological process GO terms enrichment analysis. The most enriched categories were associated with RNA polymerase activity, DNA binding and transcription (Supplementary Data 1). Moreover, we found an enrichment in biological process categories such as floral and gynoecium development, regulation of transcription and RNA processing (Supplementary Figure 2A; Supplementary Data 1).

Since SPL/NZZ binds to the DNA by its association with transcriptional factor (TF) complexes[4,5], we focused our attention on the TFs identified among the SPL/NZZ partners. We found 56 TFs as putative SPL/NZZ interactors. Quite strikingly, among the TCPs, only TCP22 was statistically enriched in our list while none of the YABBY TFs were present (Supplementary Data 1). The MADS-domain TF family was the most represented in our dataset, corresponding to almost 20% of all the TFs found (Figure 1A; Supplementary Data 1). This list of potential MADS-domain TFs interacting with SPL/NZZ included SEEDSTICK (STK), SHATTERPROOF2 (SHP2), SEPALLATA1 (SEP1), SEPALLATA2 (SEP2), SEPALLATA3 (SEP3) and AGAMOUS (AG), all proteins previously associated to ovule specification and development[21–23].

Based on these results, we verified whether SPL/NZZ could directly interact with MADS-domain TFs in yeast. Since SPL/NZZ contains an EAR-motif, which could negatively impact GAL4 transcriptional activation functionality, we used an SPL/NZZ variant lacking the EAR-motif sequence (SPL/NZZΔ). We initially tested the interaction between SPL/NZZΔ, fused with a GAL4 activation domain (AD) or DNA binding domain (BD) with AG, SEP3Δ[23] or STK. We found positive results for the SPL/NZZ$\Delta_{(AD)}$ - AG$_{(BD)}$, SPL/NZZ$\Delta_{(AD)}$ - STK$_{(BD)}$ and SEP3$\Delta_{(AD)}$ - SPL/NZZ$\Delta_{(BD)}$ interactions (Figure 1B; Supplementary Figure 2B). It was previously shown that the MADS-domain proteins generate multimeric complexes to regulate target genes[22,24]. Based on this, we performed

yeast-three-hybrid assays. We initially evaluated the formation of complexes using SPL/NZZΔ fused to the AD, SEP3Δ to the TFT and either STK or AG to the BD, finding positive results for the SPL/NZZΔ$_{(AD)}$ - SEP3Δ$_{(TFT)}$ - STK$_{(BD)}$ and SPL/NZZΔ$_{(AD)}$ - SEP3Δ$_{(TFT)}$ - AG$_{(BD)}$ interactions (Figure 1C). It is worth to notice that, even though SPL/NZZΔ$_{(AD)}$ did not directly interact with SEP3Δ$_{(BD)}$ (Supplementary Figure 2B) and only modestly with STK (Figure 1B), the presence of all three components enhanced yeast growth, suggesting the formation of a more stable complex (Figure 1C). We then tested the same interactions by fusing SPL/NZZΔ with the GAL4 BD, reconfirming the establishment of complexes with either STK and SEP3Δ or AG and SEP3Δ (Supplementary Figure 2C). Concerning the screening with SPL/NZZΔ fused with the TFT, we found that the presence of SPL/NZZΔ$_{(TFT)}$ did not enhance the already described SEP3-AG interaction[22] (Supplementary Figure 2D).

As we confirmed that SPL/NZZ can interact with the ovule identity MADS-domain TFs, we analysed STK, AG and SEP3 expression in the nucellus at stages 2-I, 2-II, concurrently with the MMC specification. STK and SEP3 were expressed in the nucellus, as shown by the study of GFP-fusion-protein reporter lines, with a pattern comparable to the one of SPL/NZZ[25–27] (Supplementary Figure 2E-H). By contrast, AG was not expressed in the nucellus (Supplementary Figure 2I, J)[27]. To further corroborate the SPL/NZZ direct interaction with SEP3 and STK we performed FRET-FLIM[28] assay in-planta. We transiently expressed in tobacco leaves SEP3Δ-GFP or STK-GFP fusion proteins either alone, or in association with SPL/NZZΔ-mCHERRY (Supplementary Figure 3). By imaging nuclei expressing solely SEP3Δ-GFP or STK-GFP we could measure, thought FLIM, a GFP lifetime of around 2,3 and 2,7 ns, respectively (Figure 1D, E; Supplementary Figure 3A-C, J-L). When SEP3Δ-GFP or STK-GFP were co-expressed with SPL/NZZΔ-mCHERRY (Supplementary Figure 3D-F, M-O), we measured a statistically significant reduction in the GFP lifetime because of FRET occurring between GFP and mCHERRY (Figure 1D, E). Since FRET could occur only when donor and acceptor proteins are at a distance lower than 10nm, these results confirm SEP3 and STK ability to physically interact with SPL/NZZ in plant cell.

It was already reported that STK-SEP3 can form a tetramer[29] while SPL/NZZ can form a homodimer[4]. Using AlphaFold3[30], we predicted *in silico* the possible formation of SEP-STK-SPL/NZZ complexes. We predicted the structure of a complex containing, respectively, two copies of SEP (1, 2, or 3), STK and SPL/NZZ. AlphaFold3 preliminary predictions could fold SPL/NZZ only from amino acid 61 to amino acids 91 forming an

alpha helix, a protein portion that contains the 8 amino acids forming the SPL-motif. Indeed, the SPL-motif was originally predicted to be part of an alpha helix spanning from amino acids 64 to amino acid 80, which has some homology to the first helix of MADS-domain TFs[2]. For these reasons, we considered only the SPL/NZZ region spanning from amino acid 61 to 91 for further predictions. All the different simulations predicted the formation of complexes with good confidence levels, assessing the reliability of the results obtained (Supplementary Figure 4A). Regarding the docking features of SPL/NZZ to the MADS-domain TFs tetramer, the different simulations indicates that SPL/NZZ contacts the K-box of STK and SEPs (Figure 1F; Supplementary Figure 4B, D). Finally, we performed binding affinity analyses [31–33], retrieving Gibbs free energy (ΔG) values and dissociation constants (K_d) that confirm the thermodynamic stability of the SPL/NZZ-MADS complexes (Figure 1G; Supplementary Figure 4C, E).

SPL/NZZ and the MADS-domain TFs share common targets

To identify the direct targets of SPL/NZZ we used the *pSPL/NZZ::SPL/NZZ:GFP AP1:GR ap1cal* line to perform a ChIP-seq experiment. Three biological replicates of inflorescence at 9 DAI were used for chromatin immunoprecipitation using an anti-GFP antibody[34,35]. After input and IP samples sequencing, peaks were considered significant with a fold enrichment (FE) > 0, FDR ≤ 0.05 and if present in at least 2 out of 3 biological replicates. This approach retrieved a list of 203 peaks, corresponding to 197 different genes (Supplementary Data 2). Around 80% of the peaks mapped in genomic regulatory regions such as promoters, supporting the reliability of the results obtained (Figure 2A). Among SPL/NZZ bound genes, we found genes previously linked to SPL/NZZ function as *ANT*[12], *YUCCA6*[36] and *PHB*[37] (Supplementary Data 2). Interestingly, also SPL/NZZ itself was present in the list, indicating the possible existence of a feedback loop involved in SPL/NZZ regulation.

SPL/NZZ does not have a DNA-binding domain. This implies that SPL/NZZ binds to its direct targets *via* TF complexes in which it is recruited. To characterise which TFs mostly relate to SPL/NZZ activity, we performed a TF DNA-motif enrichment analysis. We used the MEME suite[38] to analyse the 203 peak sequences retrieved from the SPL/NZZ ChIP-seq experiment. The only statistically enriched DNA binding site identified was the CArG-box consensus sequence, to which the MADS-domain TFs bind (Figure 2B)[39]. In addition, enrichment analysis against the Transcriptional Factor Target lists from both the AGRIS server[40–42] and the PlantGSAD database[43] revealed that SPL/NZZ targets were enriched

in genes targeted by MADS-domain TFs such as AG and SEP3 or floral homeotic factors such as APETALA2 (AP2) (Supplementary Data 2).

If SPL/NZZ binding to the DNA largely depends on its association with MADS-domain TF complexes, not only should SPL/NZZ and MADS-domain TFs target the same genes, but they should also bind these genes in the same genomic sequences. Based on this assumption, we determined the overlap of peaks obtained by the SPL/NZZ ChIP-seq with the ones obtained from a SEP3 ChIP-seq dataset[44]. The already available SEP3 ChIP-seq was performed using the same induction system and tissue used for the SPL/NZZ ChIP-seq and on a similar stage of development (8 DAI). Over 90% of SPL/NZZ peaks (185 out of 203, corresponding to 182 different genes), overlapped with peaks in the SEP3 dataset, strongly supporting the cooperation between SPL/NZZ and SEP3 for binding to the DNA, at least at the developmental stages used for the ChIP-seq experiments. (Figure 2C, D; Supplementary Data 2).

Our data indicate that SPL/NZZ could require the MADS-domain TFs SEP1, 2, and 3, as well as STK and SHPs for MMC specification. This outcome was also predictable, as it has been shown that MADS-domain TFs of classes C, D and E form multimeric complexes to establish ovule tissue and cell identity[23]. Regrettably, these transcription factors exhibit significant redundancy and multiple mutants, as the *shp1 shp2 stk ag/+* one, displays ovules homeotically changed into leaves[21–23], whereas the *sep1 sep2 sep3* mutant has all floral organs homeotically changed into sepals[45]. Therefore, to investigate the potential relevance of these MADS-domain TFs in MMC differentiation, we created a *pSPL/NZZ::MADSas* construct, to facilitate post-transcriptional gene silencing of *SEP* genes in the nucellus (Supplementary Figure 5A). We subsequently introduced this construct into *shp1/shp1 shp2/shp2 stk/STK* plants, intending to inhibit the activity of many ovule-identity MADS-domain TFs within the nucellus. We obtained three independent transformant lines expressing the *pSPL/NZZ::MADSas* (Supplementary Figure 5B). Specifically, lines 1 and 2 resulted *shp1 shp2 STK/STK,* whereas line 3 was classified as a triple *shp1 shp2 stk* mutant. Although the phenotype was much less penetrant with respect to that reported in *spl-1*, the transgenic plants *shp1 shp2 stk pSPL/NZZ::MADSas* and *shp1 shp2 STK/STK pSPL/NZZ::MADSas* showed a ratio of 25% to 45% of ovules that failed to produce the MMC (Figure 2E, F) besides an impairment in the organisation of the nucellus (Figure 2E; Supplementary Figure 5C).

Altogether, these data support that SPL/NZZ and MADS-domain TFs cooperate, forming a multimeric complex for the differentiation of the MMC.

SPL/NZZ regulates the auxin signalling network

Having identified potential direct SPL/NZZ-SEP3 target genes, we focused on their biological function to determine the mechanisms involved in the MMC differentiation. To do so, we performed a Biological Process GO terms enrichment analysis using the SPL/NZZ-SEP3 common targets (Supplementary Figure 6A; Supplementary Data 2). Besides categories associated with reproductive organs differentiation, the most enriched terms were related to auxin metabolism and biosynthesis, suggesting a direct link between SPL/NZZ and auxin (Supplementary Figure 6A; Supplementary Data 2).

To identify the genes whose expression was modified in the absence of SPL/NZZ, and the pathways associated with SPL/NZZ activity, we performed RNA sequencing on wild type (Col-0) and *spl-1* mutant pistils at stage 9[46,47]. Differential expression analysis retrieved a list of 6877 differentially expressed genes (DEGs) (FDR ≤ 0.05) (Supplementary Data 3).

We performed a Biological Process GO term enrichment analysis on the 3502 downregulated genes, revealing enrichment in terms associated with chromatin remodelling and floral development (Supplementary Figure 6B; Supplementary Data 3). By contrast, Biological Process GO term enrichment analysis done on the 3375 upregulated genes confirmed an impairment in auxin biosynthesis, metabolism and signalling (Supplementary Figure 6C; Supplementary Data 3). We also observed enrichment in categories involved in cell cycle regulation, cell wall modification and callose deposition, processes known to be required for the MMC specification[48]. To further dissect the activity of SPL/NZZ over its direct targets, we analysed the SPL/NZZ-SEP3 common target list in the light of the DEGs obtained from the *spl-1* RNA-seq. We found that 77 SPL/NZZ-SEP3 targets resulted also differentially expressed in the *spl-1* pistil with respect to the wild type (Supplementary Data 3). Nicely, these include genes involved in ovule development such as *ANT*[49], *LUG*[50], *AP2*[51], *CUC3*[52], *IPT1*[14], *SEP3*[22], *AGL15*[53] and *FUL*[54]. Interestingly, all the auxin biosynthetic genes present in the *spl-1* RNA-seq, including also the genes targeted directly by SPL/NZZ, resulted upregulated (Supplementary Data 3). Key players of auxin biosynthesis such as *YUCCA 2, 4, 6* and *TAA1*, which are normally expressed in the ovule chalaza[55], showed enhanced expression. This result is in line with SPL/NZZ proposed activity as a transcriptional repressor, which is also supported by the reduced expression of *YUC2* and *4* in the *spl-D* dominant mutant[36]. After biosynthesis in the chalaza, auxin is polarly transported towards the primordium apex mainly by PIN1, generating a region of high signalling output at the nucellus tip[55–57]. Auxin is then directed

toward the L2 layer by PIN3 and PIN1 action[57]. Since it was already reported that *PIN1* was drastically downregulated in *spl-1* ovules[14], as well as the auxin response[15], we decided to investigate in more detail auxin transport and response in wild-type and *spl-1* ovules to evaluate their impact on *spl-1* phenotype.

Focusing on wild type ovules, we observed that PIN1-GFP signal increased in the nucellus from stage 2-I, the stage in which the differentiation of the MMC initiates, to the stage 2-III, associated with the complete differentiation of the MMC (Figure 3A, B, M). Likewise, we measured a significant increase in the nucellar *DR5v2*[58] signal passing from stage 2-I to stage 2-III (Figure 3E, F, N). This dynamic in *PIN1* and *DR5v2* expression during the MMC differentiation could suggest the requirement of auxin transport and signalling to support the MMC identity acquisition. Indeed, even though we observed that PIN1-GFP accumulated similarly in wild-type and *spl-1* ovules at stage 2–I (Figure 3A, C, M), at stage 2-III, PIN1-GFP signal was drastically reduced in the *spl-1* mutant (Figure 3B, D, M), as previously shown[14,15]. Likewise, the *DR5v2* signal observed between wild type ovules at stages 2-I and 2-III (Figure 3 E-H, N) was severely reduced in in the *spl-1* background. (Figure 3 E-H, N). Besides PIN1, also PIN3 is involved in auxin transport in the nucellus. Despite this, *pPIN3::PIN3:GFP*[57,59] signal was localised at the very tip of ovule primordia in *spl-1*, and no differences were observed compared to the wild type (Supplementary Figure 7A-D).

Downregulation of *PIN1* expression and *DR5v2* response suggests that auxin is accumulated at lower levels in *spl-1* nucellus. Indeed, by using the *R2D2* reporter line[58], we detected a higher accumulation of DII-VENUS in the *spl-1* nucellus with respect to the wild type (Figure 3I-L; Supplementary Figure 7E-I).

Considering the behaviour of *PIN1* and *DR5v2*, together with the fact that auxin transport was previously suggested to be required for the MMC specification[15], we believe that *PIN1* downregulation could be the main cause of MMC absence in the *spl-1* mutant ovule.

Restoring the auxin transport is sufficient to rescue the MMC differentiation in *spl-1* ovules

Even if, molecularly, SPL/NZZ is a repressor of the transcription, during MMC differentiation, SPL/NZZ works as positive modulator of *PIN1* expression. This implies that *SPL/NZZ* activity over *PIN1* is undirect and involves, potentially, the direct targeting of negative regulators of *PIN1*. Indeed, *PIN1* was not present in the list of SPL/NZZ direct targets. Taking into consideration this information, among SPL/NZZ-SEP3 direct targets,

we searched for factors which could be genetically associated with *SPL/NZZ* activity, and which could work as intermediary of *SPL/NZZ* action over *PIN1*. During ovule patterning, SPL/NZZ was shown to be required for the repression of chalaza factors such as *ANT*, *BEL1*, *INO* and *PHB* in the nucellus[12,37,49]. As mentioned above, *ANT* is a direct target of the SPL/NZZ-MADS-domain TF complex. Particularly, in both SPL/NZZ and SEP3 ChIP-seq datasets, we found a peak containing 4 CArG-box sequences at around -3.6Kb from *ANT* TSS (Supplementary Figure 8A). Absence of SPL/NZZ function determines *ANT* ectopic expression in the nucellus[12] (Supplementary Figure 8B-I). Our attention was caught by *ANT* as a putative intermediary of *SPL/NZZ* action over *PIN1*, especially due the previous description of the ability of *ant* mutation to rescue the MMC differentiation in the *spl/nzz* background[12]. Considering the centrality of auxin transport and response for the MMC differentiation, we speculated that *ANT* could act as a repressor of *PIN1*, contributing to *PIN1* downregulation in the *spl-1* nucellus. Even though we did not find *PIN1* among ANT direct-target genes[60], we observed that *PIN1* was ectopically expressed in the chalaza and funiculus of *ant.4* mutant ovules with respect to the wild type (Supplementary Figure 8J-Q). This suggests that, in ovules, ANT acts as an indirect local repressor of *PIN1*.

Based on our present and previously reported observations[15], we hypothesised that restoring polar auxin transport in the *spl-1* ovule might be sufficient to recover the MMC differentiation. Therefore, we developed the *pSPL/NZZ::PIN1* construct, and we transformed it into *spl-1* mutant plants. Four distinct *spl-1* lines expressing the *pSPL/NZZ::PIN1* construct were characterised (Supplementary Figures 9A).

In contrast with the *spl-1* situation (Figure 4F-J, P), in *spl-1 pSPL/NZZ::PIN1,* ovule developmental defects were almost completely restored (Figure 4A-E, K-P; Supplementary Figure 9B). The MMC was correctly specified (Figure 4C, D, M, N), and completed the megasporogenesis (Figure 4E, O). Indeed, fertile ovules were formed and fertilized by pollen produced by the same plants, showing that the *pSPL/NZZ:PIN1* had rescued also the PMC defects (Supplementary Figure 9C). Interestingly, *spl-1 pSPL/NZZ:PIN1* ovules showed also a rescue of *spl-1* integuments defect (Figure 4G-J, L-O). Indeed, ovules could correctly differentiate inner and outer integuments (Figure 4G-J, L-O). Complementation of inner integuments development suggests that SPL/NZZ is important for the proper PIN1 localisation and auxin transport for inner integuments. Indeed, regulation of auxin transport was shown to be involved in integuments formation and differentiation[61]. Nevertheless, similarly to the *spl-1* mutant, the funiculus length in *spl-1 pSPL/NZZ::PIN1* ovules

remained statistically longer with respect to the wild type (Supplementary Figure 10A, B). We hypothesised that this phenotype could be related to the fact that genes involved in funiculus differentiation remained deregulated in *spl-1 pSPL/NZZ::PIN1* ovules. For instance, it was shown that *ANT* ectopic expression is directly associated with the differentiation of a longer funiculus[62]. By ISH, we observed that *ANT* remained ectopically expressed in both nucellus and funiculus of *spl-1 pSPL/NZZ::PIN1* ovules (Supplementary Figure 10C). The ectopic expression of *ANT* in *spl-1 pSPL/NZZ::PIN1* not only provide a hierarchical view in which *PIN1* is placed downstream *ANT,* but also represents a plausible explanation for the elongated funiculus of *spl-1 pSPL/NZZ::PIN1* ovules.

The inhibition of ARFs activity phenocopy the *spl-1* mutation

The results described above demonstrate the need of SPL/NZZ to regulate the auxin accumulation in the nucellus, which is essential for MMC specification. According to the auxin response model, auxin accumulation enhances Aux/IAAs degradation, releasing the ARFs from Aux/IAAs repressing activity[63]. This leads to the regulation of the expression of the ARF target genes. Based on this model, we hypothesised that the impair of the MMC differentiation in the *spl-1* mutant could be attributed to post-translational suppression of ARFs functions. Indeed, lower auxin accumulation in *spl-1* may inhibit Aux/IAAs degradation, affecting ARFs activity and thus MMC differentiation. Accordingly, ovules containing an Aux/IAA isoform resistant to the auxin-depended proteasomal degradation might mimic the *spl-1* phenotype. Single-cell RNA-seq, performed using ovules between stages 2-I and 2-III, revealed that Aux/IAAs 1, 2, 3, 4, 8, 9, 13, 16 and 26 were expressed in nucellar clusters[64]. To select the appropriate Aux/IAA to repress the ARFs activity in the nucellus, we chose the one that was previously reported to interact with several ARFs[65–67] expressed in the nucellus, and for which was available a dominant auxin-resistant allele. We choose the Aux/IAA3/SHY2[68] dominant mutant allele, named *shy2.6*[69]*. shy2.6* carries a mutation in the degron motif, impairing its ability to interact with the SCF/TIR1 complex at threshold auxin level[69], remaining constitutively bound to ARFs PB1 domain[69]. Consequently, we generate the *pSPL/NZZ::shy2.6* construct to express *shy2.6* in the nucellus of wild-type ovules.

We introduced the *pSPL/NZZ::shy2.6* construct in wild type plants, obtaining three independent lines expressing the transgene (Supplementary Figure 11A). Even if with a lower penetrance with respect to the *spl-1* mutant, in all the lines we observed an impairment in the MMC differentiation (Figure 5A-M). To confirm that the observed

phenotype was caused by the inhibition of ARFs activity rather than other factors, such as a disruption of the polar auxin transport, we examined the expression of *pPIN1::PIN1:GFP* in *pSPL/NZZ::shy2.6* plants. The expression of PIN1-GFP in *pSPL/NZZ:shy2.6* resembled that of the wild type, suggesting that the observed phenotype was probably caused by an impairment in ARFs activity (Supplementary Figure 11B-E).

ARFs activity is required for the MMC differentiation

Collectively, our data support a *scenario* in which the MMC differentiation is mediated by the post-translational regulation of the ARFs action. SHY2 is able to interact with all the classA ARFs, including ARF5/MP, ARF6, ARF7, ARF8 and ARF19. Concerning the repressor ARFs, SHY2 was shown to interact with ARF4 and ARF9[65–67]. According to a ovule single-cell RNA-seq dataset[64], *MP*, *ARF6*, *ARF8* and *ARF9* are the only SHY2-interacting ARFs expressed in the nucellus. Consequently, analysed *MP*, *ARF6*, *ARF8* and *ARF9* expression in both wild type and the *spl-1* ovules. We used previously published reporter lines to study *MP*, *ARF6* and *ARF8* domains of transcription and protein accumulation[70]. Concerning *ARF9*, as no functional protein reporter lines were available, we studied its expression pattern by *in-situ* hybridisation.

In ovule primordia, the levels of both ARF6-VENUS and ARF8-VENUS were presumably controlled at the post-translational stage, supporting previously reported observations[53] (Supplementary Figure 12E-L). Indeed, although both genes were transcribed in ovules[64] (Supplementary Figure 12E, I, G, K), ARF6 was faintly visible solely in a limited number of cells (Supplementary Figure 12F, H), while ARF8 was not visible (Supplementary Figure 12J, L). By contrast, the MP-VENUS protein accumulated in the nucellus, as previously shown[70,71] (Supplementary Figure 12A-D). The three ClassA ARFs exhibited comparable expression and protein accumulation in both wild-type and *spl-1* ovules (Supplementary Figure 12A-L). Concerning *ARF9,* we detected its transcript accumulation in both wild type and *spl-1* nucellus at stage 1-II (Supplementary Figure 13A, C). At stage 2-III, *ARF9* transcript was accumulated in the MMC and the integuments of wild-type ovules (Supplementary Figure 13B). By contrast, in the *spl-1* mutant background, *ARF9* transcript appeared miss-localised in both the nucellus and the chalaza (Supplementary Figure 13D). This could be mainly due to the fact that, in a wild-type ovule, *ARF9* transcript accumulates in the MMC and the integuments, both structures that are impaired in the *spl-1* background. Despite this, by analysing the *spl-1* RNA-seq, we observed an overall decrease in *ARF9* expression level in the *spl-1* pistil (Supplementary Data 3).

Given their expression patterns, MP and ARF9 were selected as ARFs potentially involved in the downstream auxin response, required for MMC specifications. According to our hypothesis, the absence of the MMC in the *spl-1* mutant was associated with a decrease in the nucellar auxin response, caused by the stabilisation of the Aux/IAAs and the consequential ARFs inhibition. Indeed, as previously described[63,70,72,73], ARFs activity is post-translationally regulated by the balance between ARFs and Aux/IAAs relative abundance. For this reason, we hypothesise that increase *MP* or *ARF9* levels in the *spl-1* background could overcome the repression operated by the Aux/IAAs, restoring the MMC specification. Therefore, we generated the *pSPL/NZZ::MP* and the *pSPL/NZZ::ARF9* constructs that we introduced in the *spl-1* mutant. We obtained two independent *spl-1 pSPL/NZZ::MP* lines while we found three *spl-1 pSPL/NZZ::ARF9* independent lines (Supplementary Figure 14A, B). In *spl-1 pSPL/NZZ::MP* plants, we observed that approximately 10% of ovules developed an MMC (Figure 6A-F, I). However, these cells did not undergo meiosis, suggesting only a partial acquisition of the MMC identity (Supplementary Figure 14C). By contrast, the majority of *spl-1 pSPL/NZZ::ARF9* ovules differentiated an MMC which could also proceed into sporogenesis (Figure 6G, H, J; Supplementary Figure 14D), indicating the direct involvement of ARF9 for the MMC differentiation and development.

Altogether, our results highlight the regulation of the ARFs action a key step of the SPL/NZZ downstream response during the MMC differentiation.

DISCUSSION

Although the mechanisms necessary to restrict the acquisition of the MMC identity to one single cell have been addressed[74], the regulatory network controlling the MMC specification is still largely unknown. Since SPL/NZZ is a major factor controlling MMC development, we initially focused on the identification of SPL/NZZ interacting partners *in planta.* Even though previous works highlighted the TCP TFs as the main SPL/NZZ partners[4,5], in our Co-IP/MS dataset, the MADS-domain TFs resulted the most abundant TF family. The differences in SPL/NZZ partners identified by the Co-IP/MS and by the previous screenings of SPL/NZZ interactors could be partially explained by our use of the *AP1:GR*/*ap1cal* inducible system. This system allowed us to find SPL/NZZ partners within a constrained development time window. Additionally, while our experiments were performed *in planta,* the previously reported interactors were identified by yeast-two-hybrid screening[4,5]. We identified only one TCP family member among SPL/NZZ partners. Taking

into consideration that a limited number of SPL/NZZ target genes were also identified as TCP targets (Supplementary Data 2), we suggest that complexes including SPL/NZZ and TCPs may function predominately in others developmental stages, or tissues, with respect to the ones analysed in our experiments. On the contrary, several MADS-domain transcription factors turned out to be enriched in the SPL/NZZ Co-IP/MS data. Indeed, the genomic sequences bound by SPL/NZZ-containing complexes contained the CArG-box consensus DNA sequence, typically used by MADS-domain TFs for DNA binding.

We highlighted SEP3 as a TF putatively involved in SPL/NZZ recruitment to the DNA, at least in the ovules from stage 2I to 2III, since these were the stages from which we had isolated SPL/NZZ-GFP to perform both ChIP-seq and Co-IP/MS. Indeed, SPL/NZZ shared more than 90% its targets with SEP3, and they bound these genes at the same genomic positions. To gather additional evidence supporting the cooperation of these MADS-domain TFs and SPL/NZZ in MMC specification, we developed transgenic lines exhibiting reduced expression of multiple ovule identity MADS-box genes in the SPL/NZZ expression domain. This strategy was crucial to overcome the redundancy of the ovule identity MADS-domain TFs, and because multiple mutation in these genes result in organ homeotic modifications, hindering the differentiation of ovules. Indeed, higher-order mutants such as *sep1 sep2 sep3* have flower organs converted into sepal[45] and *stk shp1 shp2 ag/+* develops leaves instead of ovules[21,23]. The transgenic plants obtained by post-transcriptionally silencing *SEPs* genes in the *shp1 shp2 stk* mutant using the *SPL/NZZ* promoter, showed ovules with defects in MMC differentiation, even if the penetrance was between 25 and 45%. In these transgenic plants, we also observed additional defects resulting from the broader role of these MADS-domain TFs in ovule differentiation and development with respect to SPL/NZZ activity (Supplementary Figure 5D).

The MADS-domain TFs STK, AG and SEP3 were shown to be fundamental for ovule development[21–23] forming complexes that regulate ovule identity. For instance, the interaction among STK, AG, SEP3 and BEL1 was described of pivotal importance to determine chalaza identity and to correctly differentiate the integuments[23]. Taking into consideration the present and the previously reported findings, it became evident that MADS-domain TF complexes interact either with SPL/NZZ or BEL1 to control the nucellar and chalazal development, respectively. Indeed, the role of SPL/NZZ in repressing chalaza identity genes in the nucellus such as *ANT*, *BEL1* and *PHB* was already reported[12,37]. At the same time, SPL/NZZ ectopic expression, was associated to the differentiation of multiple MMC-like cells[11].

We show that the key mechanism for the MMC specification likely relies on the post-translational regulation of ARFs activity, associated with the nucellar auxin accumulation.

Re-establishing the auxin transport in the *spl-1* nucellus, by expressing *PIN1* under *SPL/NZZ* promoter, was sufficient to restore the MMC differentiation and sporogenesis (Figure 7D). At the same time, the expression of the auxin-insensitive *shy2.6* mutant protein, mimicked the *spl-1* phenotype (Figure 7E). We propose that SPL/NZZ activity ensures the correct nucellar auxin level and response, by indirectly regulating the expression of *PIN1* (Figure 7A).

Likely, SPL/NZZ, acting together with SEP3 and other MADS-domain TFs, promotes *PIN1* expression by repressing *ANT* and other chalaza genes in the nucellus. According to this, *ANT* ectopic expression in the *spl/nzz* nucellus, together with other chalaza specific factors, could causes a downregulation of *PIN1* and, consequently, the impaired nucellar auxin accumulation (Figure 7B). Indeed, it was reported that the *ant* mutation partially rescues the lack of the MMC in the *spl/nzz* mutant[12], suggesting that also the nucellar auxin level could be restored in the *spl/nzz ant* double mutant (Figure 7C). To define whether *ANT* expression in the nucellus was sufficient to control *PIN1*, we transformed wild type plants with a *pSPL/NZZ::ANT* construct. Even though we obtained 3 independent lines expressing the construct (Supplementary Figure 15A), we did not observe defect in the MMC development (Supplementary Figure15B, C). This result is not unexpected since, in *spl/nzz* mutants, several genes involved in the acquisition of chalaza identity are ectopically expressed[8,12,49]. Therefore, we can conclude that SPL/NZZ is required to repress, in the nucellus, the genes required for chalaza specification and that, probably, *ANT* is only one of the genes that must be silenced to have a proper nucellus identity acquisition. Up to date, no information regarding ANT interacting partner and mode of action is available.

Even if our data support the centrality of *PIN1* action for the MMC development, it is interesting to notice that until stage 2-I, when the MMC starts its differentiation, *PIN1* expression can be observed even in the *spl-1* ovule. In the wild type, starting from stage 2-I until 2-III, the MMC undergoes to important modifications. These include a sensible enlargement in cellular and nuclear dimensions, the deposition of callose, and the expression of cellular specific markers[48]. This is associated with an increase in PIN1-GFP signal and in the nucellar auxin signalling output. By contrast, *spl-1* ovules fail in maintaining *PIN1* expression during the MMC differentiation, showing also a severely reduced auxin response. Before the start of the MMC differentiation, in the nucellus, it was

shown that one or multiple potential MMC initial are present. Over time, the nucellar phenotypic plasticity is reduced until only one MMC precursor is present, at stage 2-I [75]. The plasticity in the identification of potential MMC candidates is also supported by the eviction of the histone marker HTR13-GFP that, until stage 2-I, occurs in multiple nucellar cells. Eviction of HTR13-GFP in one single nucellar cell become prominent from stage 2-II, supporting the clear differentiation of the MMC from the other cells[76]. Despite this, it is interesting to notice that wild type and *spl-1* ovules, at precocious developmental stages, present similar phenotypes allowing the morphological identification of one or multiple potential MMC candidate cells even in the mutant background (Supplementary Figure 16A-D). This suggest that, although the MMC do not differentiate, the formation of putative MMC precursors is not affected in the *spl-1* mutant (Supplementary Figure 16A-D). According to this, the process of MMC development could be divided into two main steps: the first one would be the formation of one or multiple MMC candidates, an event which could happen independently from SPL/NZZ action. This step is limited by the reduction of the nucellar phenotypic plasticity toward the selection of one single MMC candidate that occur around stage 2-I. The second step would be the SPL/NZZ-dependent MMC identity acquisition, which starts from stage 2-I until MMC full differentiation and separation from the other nucellar cells at stage 2-III. According to this, SPL/NZZ action could be temporarily restricted during the MMC identity acquisition phase, which correspond to the step in which we observed the major changes in *PIN1* expression between wild type and *spl-1* ovules.

The regulation of *PIN1* expression during ovule development is involved in several regulatory pathways, specific for each ovule developmental phases. For instance, *PIN1* was also shown to be required to drive ovule primordia formation and outgrowth[77]. The fact that the *spl-1* mutation is not associated with alteration in ovule primordia set, strengthen the hypothesis that SPL/NZZ activity over *PIN1* is temporally restricted with the MMC specification phase.

Several factors were shown to be involved in *PIN1* regulation in the ovule. Among these, ARF17 was recently highlighted as a *PIN1* transcriptional activator[15]. Despite this, *ARF17* is repressed in the nucellus and absence of ARF17 function in the *carf17* mutant do not impact the MMC differentiation, suggesting that ARF17 action over *PIN1* is mainly in the chalaza.

Previous works already highlighted the connection between the auxin signalling and the MMC initiation. For instance, *ARF3* and *ARF17* silencing was shown to be required to repress the formation of multiple MMC cells[15,78].

According to our findings, auxin accumulation in the nucellus may trigger the degradation of the Aux/IAAs, leading to ARFs activation to support the MMC development (Figure 7A). Indeed, we observed that inhibiting the ARFs activity in a wild-type situation, by expressing the auxin-insensitive *shy2.6* mutant protein, mimicked the *spl-1* phenotype (Figure 7E). Among the ARFs expressed in the nucellus, we highlighted MP and ARF9 as putatively involved in the MMC specification. We observed that increasing *ARF9* levels could partially rescue the MMC specification in *spl-1* (Figure 7F). According to this, the MMC development might relies on the cooperation between more ARF types. Even though we focus on MP and ARF9, since they both interacts with SHY2, we could not exclude that multiple ARFs could be involved in this process. Indeed, based on ovule single-cell RNA-seq data[64], beside the ARFs previously cited, other repressor *ARFs* as *ARF1*, *ARF3*, and *ARF18* are expressed in the nucellus during the MMC differentiation, although they do not interact with SHY2. Based on our experiments, we propose that the auxin signalling, and therefore ARF action, represents the endpoint of SPL/NZZ activity. Despite this, the complete description of how ARFs promote the MMC differentiation is still hindered by the limited knowledge regarding some aspects such as, for instance, *ARF9* interacting partners and target genes. This would require additional work that we believe could represent a new and exciting field of study.

In conclusion, our data provide a regulatory mechanism (Figure 7), in which SPL/NZZ is required for the establishment of the nucellar auxin pattern, needed for the post-translational regulation of ARF TFs responsible for MMC differentiation and development. It will be of great interest to investigate the SPL/NZZ downstream network controlling PMC differentiation. Although we have not investigated this process in detail, we speculate that a similar mechanism could also control PMC specification. Although the SPL/NZZ-interacting MADS-domain partners might be different in anthers with respect to ovules, the *pSPL/NZZ::PIN1* and *pSPL/NZZ::ARF9* constructs also rescued pollen formation in the *spl-1* mutant confirming, as previously suggested[9], the importance of auxin response also for the male germline.

Acknowledgement

AC and LC were supported by MIUR PRIN2017 and PRIN2022; CA was supported by MIUR UNIMI PhD fellowship. SM was supported by postdoctoral fellowships from Fundación Alfonso Martín-Escudero (Madrid, Spain) and UNIMI. AM was supported by a predoctoral grant from UNIMI. Research in the Kaufmann lab is funded by DFG grants 512328399, 512328399, 458750707. The Kaufmann lab wishes to thank the Dresden Concept Genome Centre for support with NGS sequencing. Mass Spec was performed using a Q Exactive Plus funded by DFG (428987924). We thank Francesca Lopez for contributing to preliminary plants characterisation. We thank Stefano Buratti for technical support during the FRET-FLIM experiment. We thank Rosanna Petrella, Simona Masiero and Marta Mendes for the helpful discussion. Part of this work was performed at the Unitech NoLimits, an advance imaging facility established by the University of Milan. We thank Laura Luoni and Plant Platform, an advance facility for plant developmental studies established by the University of Milan.

Author contribution

AC, CA, SM and LC designed the research. AC, CA, GB, CS, CM, SM, AR, MS, VG, XX performed the experiments. CA, CS, AC, GB, CM, LC and KK analysed the data. AC, CA, LC, GB, CS, SM wrote the manuscript. LC and KK supported the research

Competing interest

Authors declare no competing interests

Supplementary information

Supplementary Figure 1: *pSPL/NZZ::SPL/NZZ:GFP* expression

Supplementary Figure 2: GO analysis of SPL/NZZ interactors identified by the Co-IP/MS, results of yeast-two- and three-hybrid assays and SEP3, STK and AG accumulation patterns in the ovule

Supplementary Figure 3: Single and multi-channel images showing GFP and mCHERRY signals in the nuclei represented in figure 1D

Supplementary Figure 4: AplhaFold3 predictions of SPL/NZZ-SEPs-STK complexes

Supplementary Figure 5: *MADSas* sequence homology to *SEP1, 2* and 3 and *MADSas* expression and ovule phenotypes in *pSPL/NZZ::MADSas* lines

Supplementary Figure 6: Biological processes GO terms enrichment analysis of SPL/NZZ and SEP3 common target genes and of DE genes in the *spl-1* pistil with respect to the wild type

Supplementary Figure 7: *pPIN3::PIN3:GFP* expression in wild type and *spl-1* ovules and *R2D2* signal in wild type and *spl-1* ovules at stage 1-II

Supplementary Figure 8: SPL/NZZ and SEP3 ChIP-seq peaks on *ANT* promoter, *ANT* expression in wild type and *spl-1* ovules and *PIN1* expression in wild type and *ant.4* ovules

Supplementary Figure 9: *pSPL/NZZ::PIN1* expression and ovule and anther phenotypes in *spl-1 pSPL/NZZ::PIN1* plants

Supplementary Figure 10: Funiculus length and *ANT* expression in *spl-1 pSPL/NZZ::PIN1*

Supplementary Figure 11: *pSPL/NZZ::shy2.6* expression level and PIN1-GFP accumulation in *pSPL/NZZ::shy2.6*

Supplementary Figure 12: ClassA ARFs expression in wild type and *spl-1* ovules

Supplementary Figure 13: ARF9 expression in wild type and *spl-1* ovules detected by *in-situ* hybridisation

Supplementary Figure 14: *pSPL/NZZ::MP* and *pSPL/NZZ::ARF9* expression, *spl-1 pSPL/NZZ::MP* and *spl-1 pSPL/NZZ::ARF9* ovules at stage 2-IV

Supplementary Figure 15: Expression of *pSPL/NZZ::ANT* and ovules phenotypes in *pSPL/NZZ::ANT* lines

Supplementary Figure 16: Wild type and *spl-1* ovules at precocious developmental stages

Supplementary Data 1: Results of SPL/NZZ Co-IP/MS and SPL/NZZ interactors GO terms enrichment analysis

Supplementary Data 2: Results of SPL/NZZ ChIP-seq, SPL/NZZ targets enrichment against AGRIS and PlantGSAD transcription factor target lists, SPL/NZZ ChIP-seq and SEP3 ChIP-seq peaks overlap and SPL/NZZ-SEP3 common targets GO terms enrichment analysis

Supplementary Data 3: Differentially expressed genes (DEGs) from the RNA-seq on *spl-1* vs wild type pistils, SPL/NZZ-SEP3 common targets crossed with their expression in the *spl-1* vs wild type RNA-seq, auxin biosynthetic genes expression in the *spl-1* vs wild type RNA-seq and *spl-1* vs wild type RNA-seq DEGs GO terms enrichment analysis

Supplementary Data 4: List of primers used in this study

Material and methods

Plant material and growing condition

Arabidopsis thaliana Columbia-0 plants were grown in controlled condition under a long-day photoperiod (16h light 150 µm.m^{-2}.s^{-1} / 8h dark) at 22°C. *spl-1* mutant in the Col-0 background was previously described[14]. The *pSPL/NZZ::SPL/NZZ:GFP* line was previously described[11]. The *AP1:GR/ap1cal* inducible system was described in[17]. *shp1, shp2, stk/STK* plants were described in[21]. *ant.4* mutant in the Ler background was previously described[79,80]. *pSTK:STK:GFP*, *pSEP3::SEP3:GFP, pAG::AG:GFP* were previously described[25–27]. The *spl-1 pPIN1::PIN1:GFP* line was described in[14]. *pPIN3::PIN3:GFP*[59], *DR5v2*[58] and *R2D2*[58] lines were manually crossed with *spl-1* heterozygous plants.

Generation of transgenic lines

To obtain the *pSPL/NZZ::SPL/NZZ:GFP pAP1::AP1:GR ap1cal* inducible line, *pAP1::AP1:GR ap1cal* plants[17] were transformed with the *pSPL/NZZ::SPL/NZZ:GFP* construct *via* floral dip technique using the *Agrobacterium tumefaciens* strain GV3101 .

SPL/NZZ:GFP AP1:GR ap1cal plants were induced with dexamethasone treatment directly on the inflorescence-like meristem for 9 days. After the third and the ninth dexamethasone treatment, the expression of SPL/NZZ-GFP was controlled at confocal microscope.

The *pSPL/NZZ::MADSas, pSPL/NZZ::PIN1*, *pSPL/NZZ::shy2.6*, *pSPL/NZZ::MP*, *pSPL/NZZ::ARF9* and *pSPL/NZZ::ANT* constructs were obtained with the multisite gateway cloning technique. *MADSas, PIN1*, *shy2.6*, *MP, ARF9* and *ANT* CDS sequences were amplified using the Q5 High-Fidelity DNA polymerase (NEB) and cloned into the *pDONR221* plasmid, according to the BP II protocol (Invitrogen, cat. number: 11789020). Multi-site LR reactions were performed using the *pDONR221 P1-P4* containing the *SPL/NZZ* promoter sequence[11]; the p*DONR221* containing either *MADSas, PIN1*, *shy2.6*, *MP*, *ARF9* or *ANT*; the *pDONR221 P3-P2* carrying the *SPL/NZZ 3'UTR* sequence[11] and

the destination vector *pH7m34GW*[81], according to the LR II Plus protocol (Invitrogen, cat. number: 12538120). Thanks to the floral dip technique using the *Agrobacterium tumefaciens* strain GV3101, *pSPL/NZZ::PIN1, pSPL/NZZ::MP* and *pSPL/NZZ::ARF9* were transformed into the *SPL/NZZ* spl-*1* heterozygous background. Four, two and three T2 independent transformant lines were analysed for each transformation, respectively. *pSPL/NZZ::MADSas* was transformed into the *shp1, shp2, stk/STK* background. Three T1 independent transformant lines were analysed. *pSPL/NZZ::shy2.6* and *pSPL/NZZ::ANT* were transformed into wild-type Col-0 plants. Three T1 independent transformant lines were analysed for each transformation, respectively. Primers used are listed in the Supplementary Data 4.

RT-qPCR expression analysis

For each sample, 5 inflorescences pooled together (comprising flowers spanning from stage 1 to stage 12), were used for total RNA extraction. RNA extraction was performed using the Macherey-Nagel NucleoSpin RNA plus kit (Item number: 740984.50) according to the manual instructions. 500 ng of DNA-clean total RNA for each sample were retrotranscribed using the Bio-Rad iScript™ Reverse Transcription Supermix for RT-qPCR (Bio-Rad, cat number: 1708840). cDNA was used for RT-qPCR using the Bio-Rad iTaq Universal SYBR Green Supermix (Bio-Rad, cat number: 1725120). *ACTIN8* was used as housekeeping normaliser for relative normalised expression calculation. Expression levels were expressed as mean ± SEM among three technical replicated. Primers used are listed in the Supplementary Data 4.

Analysis of ovules morphology by confocal and optical microscopy

Ovules morphology was evaluated by both confocal and optical widefield microscopy. For confocal microscopy, pistils were manually dissected from the flowers and mounted in a solution of 10 µg/ml Renaissance2200 (Renaissance Chemicals, SR2200). Samples were immediately imaged using a Nikon AX confocal microscope. Renaissance2200 was exited at 405 nm and emission signal was detected between 440-470 nm. For widefield microscopy, inflorescences were collected in a solution 9:1 ethanol/acetic acid. After 24 hours at 4°C, inflorescences were transferred to a solution 70% ethanol. Pistils were manually dissected and mounted in chloral hydrate clearing solution before microscopic imaging. Analysis of percentage of ovules developing the MMC in wild type, *spl-1,*

pSPL/NZZ::MADSas, spl-1 pSPL/NZZ::PIN1, *pSPL/NZZ::shy2.6*, *spl-1 pSPL/NZZ:MP*, *spl-1 pSPL/NZZ:ARF9* and *pSPL/NZZ::ANT* was performed on ovules at stages 2-II, 2-III.

For fluorescent reporter lines signals imaging, pistils were mounted in the Renaissance2200 solution and imaged using a Nikon AX confocal microscope. mTQ was exited with a 445nm laser and detected at 480-490nm. GFP was excited with a 488 nm laser and detected at 520-540 nm. VENUS was excited with a 514 nm laser and detected at 530-560nm. tdTOMATO was exited with a 514 nm laser and detected at 570-630 nm. Imaging was performed with sequential settings to eliminate signal crosstalk. Confocal images were analysed with the Fiji software[82]. For *PIN1-GFP* and *DR5v2* signal quantification, the Renaissance2200 channel, showing the cellular organisation, has been used to define a region of interest (ROI) comprising the whole L1 layer of the nucellus. The mean GFP and tdTOMATO signals were subsequentially measured in the ROI. The *R2D2* signal was analysed as previously described[70]. The tdTOMATO channel has been used to generate a binary mask indicating the nucellar nucelli showing *R2D2* expression. The VENUS and the tdTOMATO mean signals in the single nuclei were subsequentially measured.

Co-IP/MS material generation and data analysis

IP-MS experiments were performed as described before[20]. Essentially, nuclei were isolated from the unfixed plant tissues. Proteins, including native protein complexes, were extracted from nuclei extracts and immunoprecipitated with the GFP antibody using µMACS GFP Isolation Kit (Miltenyi Biotec, cat. number: 130-091-288). Immunoprecipitated proteins were released from the beads with 8 M urea. As control, protein extracts from before the immunoprecipitation were used and processed with the FAST method[83]. Eluted proteins were reduced with DTT, alkylated with IAA and digested with Trypsin/Lys-C Mix, Mass Spec Grade (Promega, cat. number: V5071). Resulting peptides were desalted, dried and resuspended in a loading solution. Peptide concentration was estimated using NanoDrop One A205 method. Samples were analyzed using the EASY-nLC 1200 (Thermo Fisher Scientific™) coupled to the Q Exactive Plus mass spectrometer (Thermo Fisher Scientific™). Peptides were loaded onto the Acclaim PepMap 100 C18 analytical column and separated with a linear solvent B gradient of 5% to 40 % over 70 min and 40% to 50% over 5 min. Tandem MS spectra (MS/MS) were acquired in the data-dependent acquisition (DDA) mode using a TOP15 approach.

The RAW peptide sequencing data obtained from the Q Exactive Plus were processed by the MaxQuant (version 1.6.14.0) software. Settings of the MaxQuant were mostly kept default with “label-free quantification (LFQ)”, “iBAQ” and “Match between runs” options on. The protein database was *Arabidopsis thaliana* UniProt UP000006548 without protein isoforms. After the MaxQuant analysis, the output proteinGroups.txt file was taken for further filtering and statistical analysis in the Perseus (version 1.6.15.0) software. The protein LFQ intensity data was $\log_2$-transformed. Proteins identified by only modified peptides (“Only identified by site”), by reverse sequence database (“Reverse”) and protein contaminants (“Potential Contaminant”) were removed from the analysis. Proteins with LFQ intensity values in at least two biological replicates and proteins with at least two unique peptides were kept. Missing protein LFQ intensity values were replaced only in the input samples by the imputation from the left arm of the LFQ intensity normal distribution (0.3 width, 1.8 down shift, separately for each column) to emulate background protein level. Relative protein amount differences were evaluated by two-sample t-tests with permutation-based FDR correction and S0 parameter set to 1.0. The GO term enrichment analyses were performed with clusterProfiler[84], with default parameters. The statistical significance of enriched categories was determined by the Benjamini-Hochberg (FDR) test[85], considering significant only categories with FDR ≤ 0.05. GO term enrichment analyses were performed on R studio, version 4.4.1.

ChIP-seq material generation and data analysis

ChIP-seq experiments were performed as described before[34,35]. Specifically, plant tissues were fixed in 1% formaldehyde solution, frozen in liquid nitrogen and ground to a fine powder. Nuclei were isolated through a sequential wash with buffer containing 0.5% Triton X-100 and lysed followed by chromatin sheering by sonication. After chromatin clearing, immunoprecipitation was performed with the GFP antibody (Abcam, ab290) followed by incubation with protein A magnetic beads (Thermo Fisher Scientific™, cat. number: 88845). The immunoprecipitated chromatin was released from the beads and de-crosslinked. The input sample, corresponding to the protein extract from before the immunoprecipitation, was also de-crosslinked and used as a ChIP control. The DNA was purified and concentrated using DNA Clean & Concentrator-5 kit (Zymo Research, cat. number: D4004) following manufacturer’s instructions and eluted with 20 µl of the DNA Elution Buffer. The DNA sequencing libraries for both ChIP and Input samples were prepared using ThruPLEX DNA-Seq Kit (Takara Bio, cat. number: R400674) and SMARTer DNA Unique Dual Index Kit (Takara Bio, cat. number: R400697) following manufacturer’s

instructions. DNA double size selection 100-700 bp was performed using SPRIselect beads (Beckman Coulter, cat. number: B23317). DNA libraries were sequenced on the Illumina sequencer.

Raw data were trimmed using Trimmomatic 0.39[86] with the following parameters: ILLUMINACLIP :1:30:6, LEADING: 3, TRAILING: 3, HEADCROP: 10, AVGQUAL: 20, MINLEN: 35. Mapping was performed using Bowtie 2 (version 2.5)[87] on TAIR10 genome. Duplicated reads were removed using SAMtools (version 1.7)[88]. The peak calling was performed with MACS2 (version 2.2.9.1)[89] with -g 118459858. Peaks enrichment statistical significance was evaluated according to the Benjamini-Hochberg (FDR) test. Peaks were merged using BEDTools (version 2.26.0)[90]. Only peaks present in at least 2 out of 3 biological replicates were considered. Peaks annotation was performed with ChIPseeker[91] with the following parameters: tssRegion comprised between -3000 and 0 and the genomicAnnotationPriority to 5UTR, 3UTR, Exon, Intron, Promoter, Downstream and Intergenic. The GO term enrichment analysis was performed with clusterProfiler[84], with default parameters. The statistical significance of enriched categories was determined by the Benjamini-Hochberg (FDR) test, considering significant only categories with FDR ≤ 0.05. Peak annotation and the GO term enrichment analysis were performed on R studio, version 4.4.1. The consensus sequence enrichment analysis was performed using the MEME suite [38] with default parameters. The analysis of common peaks between the SPL/NZZ ChIP-seq and the SEP3 ChIP-seq has been performed by using the command subsetByOverlaps on R studio, version 4.4.1.

In-silico prediction of protein complex structures

Protein complex structure predictions were performed with AlphaFold3 algorithm with default parameters. Protein sequences and domains annotation of SPL/NZZ (AT4G27330), STK (AT4G09960), SEP1 (AT5G15800), SEP2 (AT3G02310) and SEP3 (AT1G24260), were retrieved from the Uniprot database. AlphaFold3 models were analysed with the PyMOL software. The complexes confidence-level representations are based on the confidence files provided by AlphaFold3 algorithm. The binding-affinity analysis and the visualisation of the SPL/NZZ binding interface with the MADS tetramer was performed with the Prodigy webserver[31–33] using default parameters, at a temperature of 22°C.

RNA-seq material generation and data analysis

Three biological replicates of wild-type and *spl-1* pistils at stage 9[47] were collected in the NucleoProtect RNA (Macherey-Nagel, cat. number: 740750.500) and stored at 4°C for one day. RNA extraction was performed using the NucleoSpin RNA kit (Macherey-Nagel).

RNA was sequenced with the Novaseq X, at a depth of 30M reads with a paired-end sequencing.

Raw data were trimmed using Trimmomatic 0.39[86] with the following parameters: ILLUMINACLIP :1:30:6, LEADING: 3, TRAILING: 3, HEADCROP: 10, AVGQUAL: 20, MINLEN: 35. Mapping was performed with STAR[92], with --alignIntronMax 10000 on TAIR10 genome. Counts were obtained with featureCounts[93] (version 2.0.1), using Araport11 annotation.

Counts were filtered with HTSFilter[94] and the DEGs were obtained using DESeq2[95], considering statistically differentially expressed DEGs with an FDR ≤ 0.05, as determined by the Benjamini-Hochberg (FDR) test. The GO terms enrichment analyses were performed with clusterProfiler[84]. Only categories with an FDR ≤ 0.05, according to the Benjamini-Hochberg (FDR) test were considered statistically significant. DEGs evaluation and GO terms enrichment analyses were performed on R studio, version 4.4.1.

***In-situ* hybridisation**

In-situ hybridizations were performed as indicated in[77]. Developing inflorescences were fixed in Formaldehyde/Ethanol/Acetic Acid (3.7%/50%/5%) and embedded in paraffin. Fixed and embedded tissues were sectioned to 8 µm thickness with microtome. *PIN1*, *ANT* and *ARF9* anti-sense probes were obtained from retrotranscribed RNA extracted from wild-type inflorescences. Primer used are listed in the Supplementary Data 4.

Yeast-two- and three-hybrid assays

Yeast-two- and three-hybrid assays were performed following the protocol from[96] with some modifications.

Both yeast-two- and three-hybrid assays were performed at 28°C using a single AH109 yeast strain *via* co-transformation, or AH109 and Y187 yeast strains through co-transformation and mating.

The interactions were tested in selective media lacking leucine, tryptophan, histidine and adenine. AG and STK full-length CDS and SPL/NZZ and SEP3Δ shorter versions (SPL/NZZΔ and SEP3Δ respectively) were cloned into Gateway vector GAL4 system (pGBKT7 and pGADT7, Clontech; pTFT1[97]). Primers used are described in Supplementary Data 4.

FRET-FLIM

To test SPL/NZZ, SEP3 and STK interaction by FRET-FLIM, *SPL/NZZΔ, SEP3Δ* and *STK* CDS sequences, without the stop codons, were cloned into the *pDONR207* plasmid according to the BP II protocol (Invitrogen, cat. number: 11789020). Thanks to LR II Plus reaction (Invitrogen, cat. number: 12538120), *SEP3Δ* and *STK* CDS were introduced into the *pAB117* (provided by Rüdiger Simon, HHU Düsseldorf), which allow the C-terminus fusion of the *GFP. SPL/NZZΔ* was introduced in the *pAB118* (provided by Rüdiger Simon, HHU Düsseldorf), which allow the C-terminus fusion of the *mCHERRY. SEP3Δ* was also cloned into the *pAB119* plasmid (provided by Rüdiger Simon, HHU Düsseldorf) which allow the C-terminus fusion with both *GFP* and *mCHERRY.* Plasmids were transformed in the *Agrobacterium tumefaciens* strain GV3101. Tobacco leaf infiltration was performed as previously described[98]. The effect of Förster Resonance Energy Transfer (FRET) between GFP and mCHERRY was measured by fluorescence lifetime imaging (FLIM) of the GFP, using a Nikon ECLIPSE Ni-E A1 confocal equipped with a pulsed laser at 485nm and taking advantage of the SymPhoTime 64 software (PicoQuant, https://www.picoquant.com/). Each acquisition has been performed reaching a photon count per pixel spanning from 30 to 50. Acquisition of coumarin6 (0.1mM EtOH 100%), was used as reference. Coumarin6 has excitation and emission spectra similar to the GFP ones and has a known photon lifetime of around 2.5 ns. The evaluation of its decay was used, through a phasor transformation function, to calculate the Instrument Response. The FLIM results obtained by the SymPhoTime 64 software were corrected with the Instrument Response thanks to the FLIM-Phasor analysis software[99] (FlimLabs, https://www.flimlabs.com) generating a phasor plot in which the different pixels of an image are clustered in relation to their lifetime. This step allows the identification of the nuclei and the evaluation of the GFP photon decay.

Statistical information

The SPL/NZZ Co-IP/MS experiment has been performed on three independent biological replicates of *pSPL/NZZ::SPL/NZZ:GFP pAP1::AP1:GR ap1cal* inflorescences at 9 DAI. Proteins with LFQ intensity values in 2 out of 3 biological replicates and with at least two unique peptides were kept. Relative protein amount differences were evaluated by two-sample t-tests with permutation-based FDR correction and S0 parameter set to 1.0.

The SPL/NZZ ChIP-seq experiment has been performed on three independent biological replicates of *pSPL/NZZ::SPL/NZZ:GFP pAP1::AP1:GR ap1cal* inflorescences at 9 DAI. Peaks with an FDR ≤ 0.05 and present in at least 2 out of 3 biological replicates were considered. Statistical significance was evaluated according to the Benjamini-Hochberg (FDR) test.

Statistical significance of SPL/NZZ target genes enrichment against AGRIS and PlantGSAD transcriptional factor target lists has been evaluated with the ShinyGo[100] webtool, and only categories with an FDR ≤ 0.05 were considered significant.

The *spl-1* vs wild type RNA-seq experiment has been performed on three independent biological replicates of wild type and *spl-1* pistils at stage 9 of development. Statistical significance of *spl-1* vs wild-type DEGs was evaluated with the Benjamini-Hochberg (FDR) test and only genes with an FDR ≤ 0.05 were considered significant.

Statistical significance of Gene Ontology enrichment analyses on the results obtained from the SPL/NZZ Co-IP/MS, the SPL/NZZ ChIP-seq and the *spl-1* vs wild type RNA-seq, was evaluated according to the Benjamini-Hochberg (FDR) test. Categories with an FDR ≤ 0.05 were considered significant.

In the FRET-FLIM experiment to test the SEP3-SPL/NZZ interaction, statistical significance of the reduction in the GFP lifetime has been evaluated according to the results the student's t-test, two-tailed distribution homoscedastic, confronting the GFP lifetime in nuclei expressing SEP3Δ-GFP with the one measured in nuclei expressing SEP3Δ-GFP + SPL/NZZΔ-mCHERRY. The comparison between SEP3Δ-GFP and SEP3Δ-GFP-mCHERRY has been used as a positive control for the experiment. Comparisons with a $p \leq 0.05$ were considered significant. student's t-test calculation has been performed with Microsoft Excell. In the FRET-FLIM experiment to test the STK-SPL/NZZ interaction, statistical significance of the reduction in the GFP lifetime has been evaluated according to the results the student's t-test, two-tailed distribution homoscedastic, confronting the GFP lifetime in nuclei expressing STK-GFP with the one measured in nuclei expressing STK-GFP + SPL/NZZΔ-mCHERRY. The comparison between SEP3Δ-GFP and SEP3Δ-GFP-mCHERRY has been used as a positive control for the experiment. Comparisons with a $p \leq 0.05$ were considered significant. student's t-test calculation has been performed with Microsoft Excell. For *PIN1-GFP*, *DR5v2* and *R2D2* signal intensity measurements, statistical significance has been evaluated according to the results the student's t-test, two-tailed distribution homoscedastic, confronting the mutant with the wild-type. Comparisons with a $p \leq 0.05$ were considered

significant. student's t-test calculation has been performed with Microsoft Excell. For the morphological analyses of ovules differentiating an MMC, as well as funiculus length measurements, statistical significance has been evaluated according to the results of one-way ANOVA with post-hoc Tukey HSD test. Comparisons with a $p \leq 0.05$ were considered significant. The analysis has been performed with the webtool: https://astatsa.com/OneWay_Anova_with_TukeyHSD/.

Data availability statement

All materials reported in this study are available from the corresponding author upon request. Co-IP/MS raw data can be found under the accession XXX. ChIP-seq raw data can be found under the accession XXX. RNA-seq raw data can be found under the accession XXX. Lists of SPL/NZZ interactors and target genes, as well as differentially expressed genes in *spl-1* with respect to the wild type, can be found in the Supplementary Data 1-3. Primers used are listed in the Supplementary Data 4.

References

1. Schiefthaler, U. *et al.* Molecular analysis of NOZZLE, a gene involved in pattern formation and early sporogenesis during sex organ development in Arabidopsis thaliana. *Proc. Natl. Acad. Sci. U. S. A.* **96**, 11664–11669 (1999).
2. Yang, W. C., Ye, D., Xu, J. & Sundaresan, V. The SPOROCYTELESS gene of Arabidopsis is required for initiation of sporogenesis and encodes a novel nuclear protein. *Genes Dev.* **13**, 2108–2117 (1999).
3. Tao, Q. *et al.* The TIE1 transcriptional repressor links TCP transcription factors with TOPLESS/TOPLESS-RELATED corepressors and modulates leaf development in Arabidopsis. *Plant Cell* **25**, 421–437 (2013).
4. Chen, G.-H., Sun, J.-Y., Liu, M., Liu, J. & Yang, W.-C. SPOROCYTELESS Is a Novel Embryophyte-Specific Transcription Repressor that Interacts with TPL and TCP Proteins in Arabidopsis. *J. Genet. Genomics* **41**, 617–625 (2014).
5. Wei, B. *et al.* The molecular mechanism of SPOROCYTELESS/NOZZLE in controlling Arabidopsis ovule development. *Cell Res.* **25**, 121–134 (2015).
6. Szemenyei, H., Hannon, M. & Long, J. A. TOPLESS mediates auxin-dependent transcriptional repression during Arabidopsis embryogenesis. *Science (80-.).* **319**, 1384–1386 (2008).
7. Wang, L., Kim, J. & Somers, D. E. Transcriptional corepressor TOPLESS complexes

with pseudoresponse regulator proteins and histone deacetylases to regulate circadian transcription. *Proc. Natl. Acad. Sci. U. S. A.* **110**, 761–766 (2013).

8. Sieber, P., Petrascheck, M., Barberis, A. & Schneitz, K. Organ polarity in Arabidopsis. NOZZLE physically interacts with members of the YABBY family. *Plant Physiol.* **135**, 2172–2185 (2004).
9. Zheng, Y. *et al.* Auxin guides germ-cell specification in Arabidopsis anthers. *Proc. Natl. Acad. Sci. U. S. A.* **118**, (2021).
10. Ito, T. *et al.* The homeotic protein AGAMOUS controls microsporogenesis by regulation of SPOROCYTELESS. *Nature* **430**, 356–360 (2004).
11. Mendes, M. A. *et al.* The RNA-dependent DNA methylation pathway is required to restrict SPOROCYTELESS/NOZZLE expression to specify a single female germ cell precursor in Arabidopsis. *Development* **147**, (2020).
12. Balasubramanian, S. & Schneitz, K. NOZZLE regulates proximal-distal pattern formation, cell proliferation and early sporogenesis during ovule development in Arabidopsis thaliana. *Development* **127**, 4227–4238 (2000).
13. Schneitz, K., Baker, S. C., Gasser, C. S. & Redweik, A. Pattern formation and growth during floral organogenesis: HUELLENLOS and AINTEGUMENTA are required for the formation of the proximal region of the ovule primordium in Arabidopsis thaliana. *Development* **125**, 2555–2563 (1998).
14. Bencivenga, S., Simonini, S., Benková, E. & Colombo, L. The transcription factors BEL1 and SPL are required for cytokinin and auxin signaling during ovule development in Arabidopsis. *Plant Cell* **24**, 2886–2897 (2012).
15. Huang, J. *et al.* Specification of female germline by microRNA orchestrated auxin signaling in Arabidopsis. *Nat. Commun.* **13**, 1–14 (2022).
16. Vijayan, A. *et al.* A digital 3D reference atlas reveals cellular growth patterns shaping the arabidopsis ovule. *Elife* **10**, 1–38 (2021).
17. O'Maoiléidigh, D. S. & Wellmer, F. A floral induction system for the study of early Arabidopsis flower development. *Methods Mol. Biol.* **1110**, 307–314 (2014).
18. Ó'Maoiléidigh, D. S. *et al.* Control of reproductive floral organ identity specification in arabidopsis by the C function regulator AGAMOUS. *Plant Cell* **25**, 2482–2503 (2013).
19. Zhao, F. *et al.* Phosphorylation of SPOROCYTELESS/NOZZLE by the MPK3/6 Kinase Is Required for Anther Development. *Plant Physiol.* **173**, 2265–2277 (2017).
20. Smaczniak, C. Immunoprecipitation-Mass Spectrometry (IP-MS) of Protein-Protein

Interactions of Nuclear-Localized Plant Proteins. *Methods Mol. Biol.* **2698**, 163–181 (2023).

21. Pinyopich, A. *et al.* Assessing the redundancy of MADS-box genes during carpel and ovule development. *Nature* **424**, 85–88 (2003).
22. Favaro, R. *et al.* MADS-box protein complexes control carpel and ovule development in Arabidopsis. *Plant Cell* **15**, 2603–2611 (2003).
23. Brambilla, V. *et al.* Genetic and molecular interactions between BELL1 and MADS box factors support ovule development in Arabidopsis. *Plant Cell* **19**, 2544–2556 (2007).
24. Espinosa-Soto, C., Immink, R. G. H., Angenent, G. C., Alvarez-Buylla, E. R. & de Folter, S. Tetramer formation in Arabidopsis MADS domain proteins: analysis of a protein-protein interaction network. *BMC Syst. Biol.* **8**, 9 (2014).
25. Mizzotti, C. *et al.* SEEDSTICK is a master regulator of development and metabolism in the Arabidopsis seed coat. *PLoS Genet.* **10**, e1004856 (2014).
26. Smaczniak, C. *et al.* Characterization of MADS-domain transcription factor complexes in Arabidopsis flower development. *Proc. Natl. Acad. Sci. U. S. A.* **109**, 1560–1565 (2012).
27. Urbanus, S. L. *et al.* In planta localisation patterns of MADS domain proteins during floral development in Arabidopsis thaliana. *BMC Plant Biol.* **9**, 1–16 (2009).
28. Somssich, M. & Simon, R. Studying Protein–Protein Interactions In Planta Using Advanced Fluorescence Microscopy BT - Plant Genomics: Methods and Protocols. in (ed. Busch, W.) 267–285 (Springer New York, New York, NY, 2017). doi:10.1007/978-1-4939-7003-2_17.
29. Mendes, M. A. *et al.* MADS Domain Transcription Factors Mediate Short-Range DNA Looping That Is Essential for Target Gene Expression in Arabidopsis . *Plant Cell* **25**, 2560–2572 (2013).
30. Abramson, J. *et al.* Accurate structure prediction of biomolecular interactions with AlphaFold 3. *Nature* **630**, 493–500 (2024).
31. Honorato, R. V *et al.* Structural Biology in the Clouds: The WeNMR-EOSC Ecosystem. *Front. Mol. Biosci.* **8**, 729513 (2021).
32. Xue, L. C., Rodrigues, J. P., Kastritis, P. L., Bonvin, A. M. & Vangone, A. PRODIGY: a web server for predicting the binding affinity of protein–protein complexes. *Bioinformatics* **32**, 3676–3678 (2016).
33. Vangone, A. & Bonvin, A. M. J. J. Contacts-based prediction of binding affinity in

protein–protein complexes. *Elife* **4**, e07454 (2015).

34. van Mourik, H., Muiño, J. M., Pajoro, A., Angenent, G. C. & Kaufmann, K. Characterization of in vivo DNA-binding events of plant transcription factors by ChIP-seq: experimental protocol and computational analysis. *Methods Mol. Biol.* **1284**, 93–121 (2015).

35. Kaufmann, K. *et al.* Chromatin immunoprecipitation (ChIP) of plant transcription factors followed by sequencing (ChIP-SEQ) or hybridization to whole genome arrays (ChIP-CHIP). *Nat. Protoc.* **5**, 457–472 (2010).

36. Li, L.-C. *et al.* SPOROCYTELESS modulates YUCCA expression to regulate the development of lateral organs in Arabidopsis. *New Phytol.* **179**, 751–764 (2008).

37. Sieber, P. *et al.* Pattern formation during early ovule development in Arabidopsis thaliana. *Dev. Biol.* **273**, 321–334 (2004).

38. Bailey, T. L. *et al.* MEME SUITE: tools for motif discovery and searching. *Nucleic Acids Res.* **37**, W202-8 (2009).

39. Folter, S. de & Angenent, G. C. trans meets cis in MADS science. *Trends Plant Sci.* **11**, 224–231 (2006).

40. Yilmaz, A. *et al.* AGRIS: the Arabidopsis Gene Regulatory Information Server, an update. *Nucleic Acids Res.* **39**, D1118–D1122 (2011).

41. Palaniswamy, S. K. *et al.* AGRIS and AtRegNet. a platform to link cis-regulatory elements and transcription factors into regulatory networks. *Plant Physiol.* **140**, 818–829 (2006).

42. Davuluri, R. V *et al.* AGRIS: Arabidopsis Gene Regulatory Information Server, an information resource of Arabidopsis cis-regulatory elements and transcription factors. *BMC Bioinformatics* **4**, 25 (2003).

43. Ma, X. *et al.* PlantGSAD: a comprehensive gene set annotation database for plant species. *Nucleic Acids Res.* **50**, D1456–D1467 (2022).

44. Pajoro, A. *et al.* Dynamics of chromatin accessibility and gene regulation by MADS-domain transcription factors in flower development. *Genome Biol.* **15**, R41 (2014).

45. Pelaz, S., Ditta, G. S., Baumann, E., Wisman, E. & Yanofsky, M. F. B and C floral organ identity functions require SEPALLATA MADS-box genes. *Nature* **405**, 200–203 (2000).

46. Manrique, S. *et al.* HISTONE DEACETYLASE19 Controls Ovule Number Determination and Transmitting Tract Differentiation. *Plant Physiol.* **194**, 2117–2135 (2024).

47. Smyth, D. R., Bowman, J. L. & Meyerowitz, E. M. Early flower development in Arabidopsis. *Plant Cell* **2**, 755–767 (1990).
48. Pinto, S. C. *et al.* Germline β-1,3-glucan deposits are required for female gametogenesis in Arabidopsis thaliana. *Nat. Commun.* **15**, 5875 (2024).
49. Balasubramanian, S. & Schneitz, K. NOZZLE links proximal-distal and adaxial-abaxial pattern formation during ovule development in Arabidopsis thaliana. *Development* **129**, 4291–4300 (2002).
50. Liu, Z., Franks, R. G. & Klink, V. P. Regulation of Gynoecium Marginal Tissue Formation by LEUNIG and AINTEGUMENTA. *Plant Cell* **12**, 1879 (2000).
51. Byzova, M. V. *et al.* Arabidopsis STERILE APETALA, a multifunctional gene regulating inflorescence, flower, and ovule development. *Genes Dev.* **13**, 1002–1014 (1999).
52. Galbiati, F. *et al.* An integrative model of the control of ovule primordia formation. *Plant J.* **76**, 446–455 (2013).
53. Fernandez, D. E. *et al.* The embryo MADS domain factor AGL15 acts postembryonically: Inhibition of perianth senescence and abscission via constitutive expression. *Plant Cell* **12**, 183–197 (2000).
54. Ferrándiz, C., Gu, Q., Martienssen, R. & Yanofsky, M. F. Redundant regulation of meristem identity and plant architecture by FRUITFULL, APETALA1 and CAULIFLOWER Cristina. **734**, 725–734 (2000).
55. Robert, H. S., Crhak Khaitova, L., Mroue, S. & Benková, E. The importance of localized auxin production for morphogenesis of reproductive organs and embryos in Arabidopsis. *J. Exp. Bot.* **66**, 5029–5042 (2015).
56. Benková, E. *et al.* Local, Efflux-Dependent Auxin Gradients as a Common Module for Plant Organ Formation. *Cell* **115**, 591–602 (2003).
57. Ceccato, L. *et al.* Maternal Control of PIN1 Is Required for Female Gametophyte Development in Arabidopsis. *PLoS One* **8**, 2–8 (2013).
58. Liao, C.-Y. *et al.* Reporters for sensitive and quantitative measurement of auxin response. *Nat Meth* **12**, 207–210 (2015).
59. Zádníková, P. *et al.* Role of PIN-mediated auxin efflux in apical hook development of Arabidopsis thaliana. *Development* **137**, 607–617 (2010).
60. Krizek, B. A., Blakley, I. C., Ho, Y.-Y., Freese, N. & Loraine, A. E. The Arabidopsis transcription factor AINTEGUMENTA orchestrates patterning genes and auxin signaling in the establishment of floral growth and form. *Plant J.* **103**, 752–768

(2020).

61. Kelley, D. R., Arreola, A., Gallagher, T. L. & Gasser, C. S. ETTIN (ARF3) physically interacts with KANADI proteins to form a functional complex essential for integument development and polarity determination in Arabidopsis. *Development* **139**, 1105–1109 (2012).

62. Krizek, B. A. Ectopic expression of AINTEGUMENTA in Arabidopsis plants results in increased growth of floral organs. *Dev. Genet.* **25**, 224–236 (1999).

63. Weijers, D. & Wagner, D. Transcriptional Responses to the Auxin Hormone. *Annu. Rev. Plant Biol.* **67**, 539–574 (2016).

64. Hou, Z. *et al.* High-throughput single-cell transcriptomics reveals the female germline differentiation trajectory in Arabidopsis thaliana. *Commun. Biol.* **4**, 1149 (2021).

65. Piya, S., Shrestha, S. K., Binder, B., Neal Stewart, C. & Hewezi, T. Protein-protein interaction and gene co-expression maps of ARFs and Aux/IAAs in Arabidopsis. *Front. Plant Sci.* **5**, 1–9 (2014).

66. Vernoux, T. *et al.* The auxin signalling network translates dynamic input into robust patterning at the shoot apex. *Mol. Syst. Biol.* **7**, (2011).

67. Wanamaker, S. A. *et al.* CrY2H-seq: a massively multiplexed assay for deep-coverage interactome mapping. *Nat. Methods* **14**, 819–825 (2017).

68. Tian, Q., Uhlir, N. J. & Reed, J. W. Arabidopsis SHY2/IAA3 Inhibits Auxin-Regulated Gene Expression. *Plant Cell* **14**, 301–319 (2002).

69. Knox, K., Grierson, C. S. & Leyser, O. AXR3 and SHY2 interact to regulate root hair development. *Development* **130**, 5769–5777 (2003).

70. Cavalleri, A. *et al.* Auxin-dependent post-translational regulation of MONOPTEROS in the Arabidopsis root. *Cell Rep.* **43**, 115083 (2024).

71. Cucinotta, M. *et al.* Alternative Splicing Generates a MONOPTEROS Isoform Required for Ovule Development. *Curr. Biol.* **31**, 892-899.e3 (2021).

72. Chandler, J. W. Auxin response factors. *Plant Cell Environ.* **39**, 1014–1028 (2016).

73. Guilfoyle, T. J. The PB1 domain in auxin response factor and aux/IAA proteins: A versatile protein interaction module in the auxin response. *Plant Cell* **27**, 33–43 (2015).

74. Pinto, S. C., Mendes, M. A., Coimbra, S. & Tucker, M. R. Revisiting the Female Germline and Its Expanding Toolbox. *Trends Plant Sci.* **24**, 455–467 (2019).

75. Hernandez-Lagana, E. *et al.* Organ geometry channels reproductive cell fate in the Arabidopsis ovule primordium. *Elife* **10**, (2021).

76. Hernandez-lagana, E. & Autran, D. H3.1 Eviction Marks Female Germline Precursors in Arabidopsis. 1–8 (2020).
77. Galbiati, F. *et al.* An integrative model of the control of ovule primordia formation. *Plant J.* **76**, 446–455 (2013).
78. Su, Z. *et al.* The THO Complex Non-Cell-Autonomously Represses Female Germline Specification through the TAS3-ARF3 Module. *Curr. Biol.* **27**, 1597-1609.e2 (2017).
79. Losa, A., Colombo, M., Brambilla, V. & Colombo, L. Genetic interaction between AINTEGUMENTA (ANT) and the ovule identity genes SEEDSTICK (STK), SHATTERPROOF1 (SHP1) and SHATTERPROOF2 (SHP2). *Sex. Plant Reprod.* **23**, 115–121 (2010).
80. Baker, S. C., Robinson-Beers, K., Villanueva, J. M., Gaiser, J. C. & Gasser, C. S. Interactions among genes regulating ovule development in Arabidopsis thaliana. *Genetics* **145**, 1109–1124 (1997).
81. Karimi, M., De Meyer, B. & Hilson, P. Modular cloning in plant cells. *Trends Plant Sci.* **10**, 103–105 (2005).
82. Schindelin, J. *et al.* Fiji: An open-source platform for biological-image analysis. *Nat. Methods* **9**, 676–682 (2012).
83. Wiśniewski, J. R., Zougman, A., Nagaraj, N. & Mann, M. Universal sample preparation method for proteome analysis. *Nat. Methods* **6**, 359–362 (2009).
84. Yu, G., Wang, L.-G., Han, Y. & He, Q.-Y. clusterProfiler: an R package for comparing biological themes among gene clusters. *OMICS* **16**, 284–287 (2012).
85. Benjamini, Y. & Hochberg, Y. Controlling the False Discovery Rate: A Practical and Powerful Approach to Multiple Testing. *J. R. Stat. Soc. Ser. B* **57**, 289–300 (1995).
86. Bolger, A. M., Lohse, M. & Usadel, B. Trimmomatic: A flexible trimmer for Illumina sequence data. *Bioinformatics* **30**, 2114–2120 (2014).
87. Langmead, B. & Salzberg, S. L. Fast gapped-read alignment with Bowtie 2. *Nat. Methods* **9**, 357–359 (2012).
88. Li, H. *et al.* The Sequence Alignment/Map format and SAMtools. *Bioinformatics* **25**, 2078–2079 (2009).
89. Zhang, Y. *et al.* Model-based Analysis of ChIP-Seq (MACS). *Genome Biol.* **9**, R137 (2008).
90. Quinlan, A. R. & Hall, I. M. BEDTools: a flexible suite of utilities for comparing genomic features. *Bioinformatics* **26**, 841–842 (2010).

91. Yu, G., Wang, L.-G. & He, Q.-Y. ChIPseeker: an R/Bioconductor package for ChIP peak annotation, comparison and visualization. *Bioinformatics* **31**, 2382–2383 (2015).
92. Dobin, A. *et al.* STAR: ultrafast universal RNA-seq aligner. *Bioinformatics* **29**, 15–21 (2013).
93. Liao, Y., Smyth, G. K. & Shi, W. featureCounts: an efficient general purpose program for assigning sequence reads to genomic features. *Bioinformatics* **30**, 923–930 (2014).
94. Rau, A., Gallopin, M., Celeux, G. & Jaffrézic, F. Data-based filtering for replicated high-throughput transcriptome sequencing experiments. *Bioinformatics* **29**, 2146–2152 (2013).
95. Love, M. I., Huber, W. & Anders, S. Moderated estimation of fold change and dispersion for RNA-seq data with DESeq2. *Genome Biol.* **15**, 1–21 (2014).
96. Gietz, D., Jean, A. S., Woods, R. A. & Schiestl, R. H. Improved method for high efficiency transformation of intact yeast cells. *Nucleic Acids Res.* **20**, 1425 (1992).
97. Gutierrez-Cortines, M. E. & Davies, B. Beyond the ABCS: Ternary complex formation in the control of floral organ identity. *Trends Plant Sci.* **5**, 471–476 (2000).
98. Costa, A. *et al.* Ca2+-dependent phosphoregulation of the plasma membrane Ca2+-ATPase ACA8 modulates stimulus-induced calcium signatures. *J. Exp. Bot.* **68**, 3215–3230 (2017).
99. Vallmitjana, A. *et al.* GSLab: open-source platform for advanced phasor analysis in fluorescence microscopy. *Bioinformatics* **41**, (2025).
100. Ge, S. X., Jung, D., Jung, D. & Yao, R. ShinyGO: A graphical gene-set enrichment tool for animals and plants. *Bioinformatics* **36**, 2628–2629 (2020).

Figures

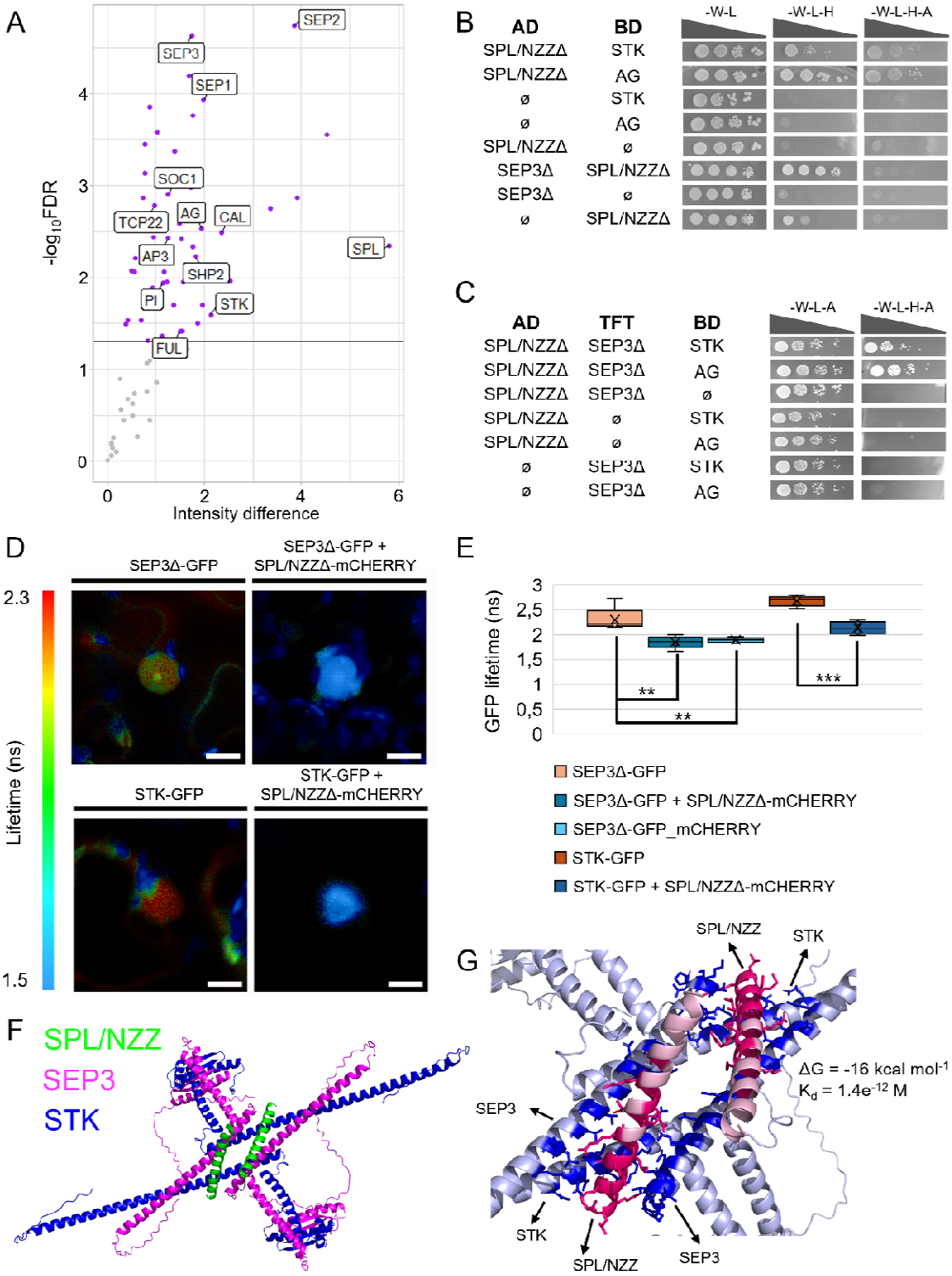

Figure 1. SPL/NZZ directly interacts with MADS-domain TFs. (**A**) Vulcano plot showing, with purple dots, the TFs statistically enriched in the SPL/NZZ Co-IP/MS dataset. MADS-domain TFs, SPL/NZZ and TCP22 have been highlighted with labels. The experiment has been performed using three independent biological replicates of *SPL/NZZ:GFP AP1:GR ap1cal* inflorescences at 9 DAI. Proteins with a positive enrichment

($\log_2$ Intensity difference > 0) and FDR ≤ 0.05 were considered significant. (**B**) SPL/NZZ-MADS-domain TFs (AG, STK and SEP3) direct interaction by yeast-two-hybrid assay. Interactions are tested on media depleted of histidine (-W -L -H), or histidine and adenine (-W -L -H -A). For each interaction on the different media, yeast has been spotted at four different concentrations according to a serial dilution (OD 0.5; 1:10; 1:100; 1:1000). (**C**) SPL/NZZ form complexes with STK, SEP3 and AG by yeast-three-hybrid assays. Interactions are tested on a medium depleted of histidine (-W -L -H -A). For each interaction, yeast has been spotted at four different concentrations according to a serial dilution (OD 0.5; 1:10; 1:100; 1:1000). (**D**, **E**) SPL/NZZ interaction with SEP3 and STK tested by FRET-FLIM. The GFP signal imaged from nuclei expressing SEP3Δ-GFP or STK-GFP fusion proteins, either alone or together with the SPL/NZZΔ-mCHERRY fusion protein, is represented according to the GFP Lifetime (**D**). The original images of the different nuclei can be found in the Supplementary Figure 3. (**E**) Box plot representing the GFP lifetime of nuclei expressing SEP3Δ-GFP, SEP3Δ-GFP + SPL/NZZΔ-mCHERRY, STK-GFP and STK-GFP + SPL/NZZΔ-mCHERRY, as calculated by FILM combined with a phasor plot to distinguish different lifetime populations. The SEP3Δ-GFP-mCHERRY fusion protein has been used as a positive control. In this case, FRET between GFP and mCHERRY should occur with the maximum efficiency. Measurements have been performed on 5, 5, 5, 11 and 5 different nuclei expressing SEP3Δ-GFP, SEP3Δ-GFP + SPL/NZZΔ-mCHERRY, SEP3Δ-GFP-mCHERRY, STK-GFP and STK-GFP + SPL/NZZΔ-mCHERRY respectively. Asterisks over boxes represent the statistical significance as determined by student's t-test, two-tailed distribution homoscedastic, confronting SEP3Δ-GFP with SEP3Δ-GFP + SPL/NZZΔ-mCHERRY and SEP3Δ-GFP-mCHERRY, or STK-GFP with STK-GFP + SPL/NZZΔ-mCHERRY. ** = $p \leq 0.01$; *** = $p \leq 0.001$. Box-plots elements correspond to: centre line = median; X = average; box limits = interquartile range; whiskers = lowest and highest values in the 1.5 interquartile range. Single measures are represented with dots in the boxes. Scale Bars: 10 µm. (**F**) AlphaFold3 predictions of the SPL/NZZ, SEP3 and STK complex. Two copies of STK are shown in blue, two copies of SEP3 are shown in magenta and two copies of SPL/NZZ aa61-91 are shown in green. (**G**) Close-up view of the SPL/NZZ-SEP3-STK complex according to a binding-affinity prediction. The coloured portion on the complex contains 121 intermolecular contacts between SPL/NZZ and the STK-SEP3 at a maximum distance of 5.5 Å. Particularly, STK and SEP3 amino acids that take contact with SPL/NZZ are showed in blue. SPL/NZZ amino acids that participate in binding to STK and SEP3 are

depicted in red. Light blue and light red colouring marks regions where there is no binding. It is possible to notice that one SPL/NZZ molecule interacts with the K-domain of one STK molecule and two SEP3 molecules. The Gibbs free energy (ΔG) for this complex is -16.0 kcal mol^{-1} and the dissociation constant (K_d) is 1.4 e^{-12} M.

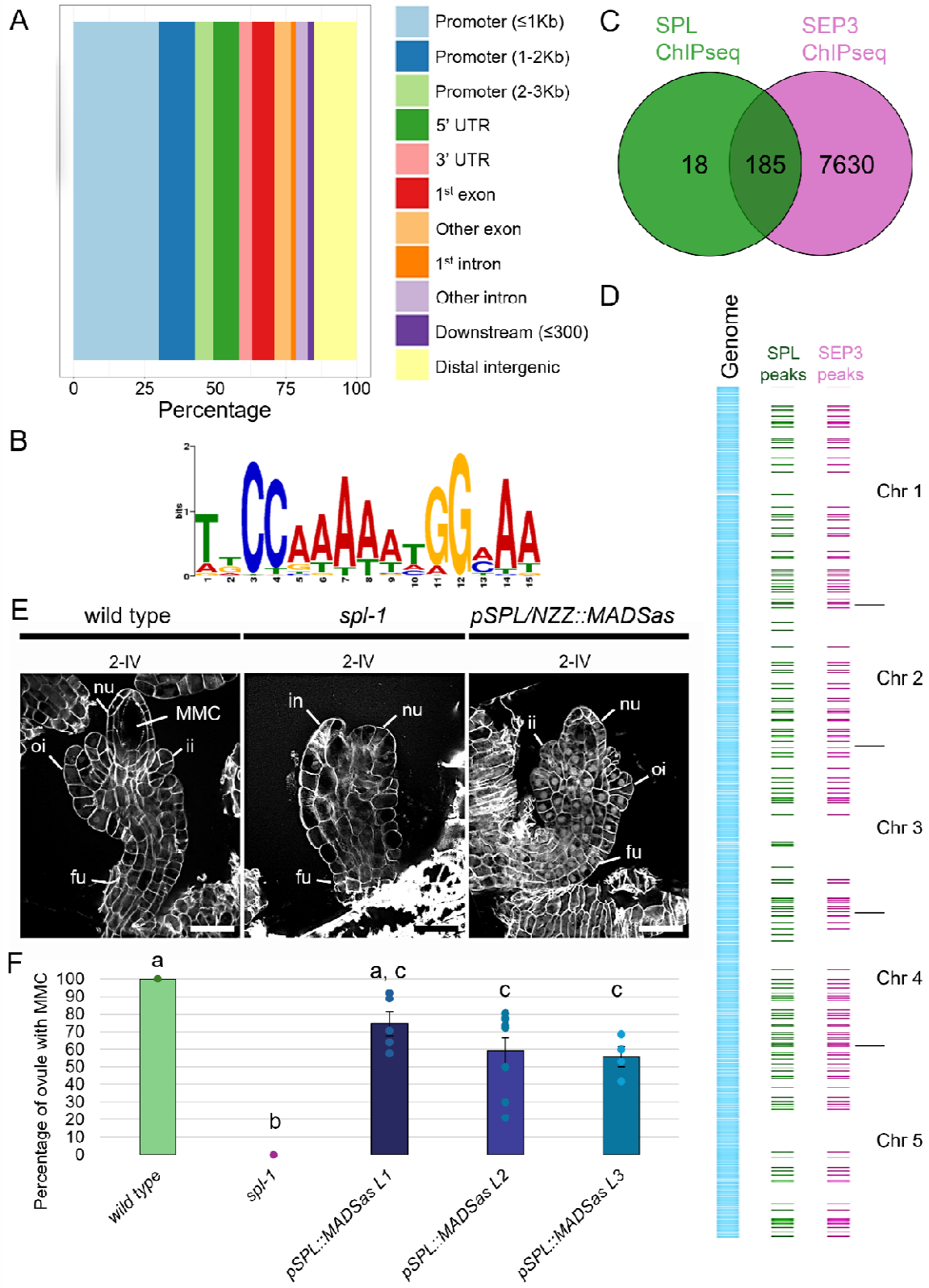

Figure 2: SPL/NZZ direct target genes are shared with MADS-domain TFs. (**A**) Bar plot showing the SPL/NZZ ChIP-seq peaks localisation along the genome. Around the

80% of the identified peaks falls in transcriptional regulatory sequences, such as promoter, 5' UTR, first exon, first intron and 3' UTR. The experiment has been performed on three biological replicates of *SPL/NZZ:GFP AP1:GR ap1cal* inflorescences at 9 DAI. Peaks were considered significant with FE> 0, FDR ≤ 0.05 and if present in at least 2 biological replicates out of 3. (**B**) The CArG-box motif is the only enriched TF DNA sequence binding-site identified among the SPL/NZZ ChIP-seq peaks. The analysis has been performed with the XTREME tool from the MEME suite. (**C**) Venn diagram showing the intersection between the SPL/NZZ ChIP-seq peaks and the SEP3 ChIP-seq peaks. 185 SPL/NZZ peaks, representing more than 90% of the total peaks, are overlapping with SEP3 peaks. (**D**) SPL/NZZ ChIP-seq and SEP3 ChIP-seq overlapping peaks visualisation along the *A. thaliana* genome. All the significant SPL/NZZ ChIP-seq peaks are visualized in green. SEP3 ChIP-seq peaks overlapping with SPL/NZZ ones are shown in magenta. (**E**) wild type, *spl-1* and *pSPL/NZZ::MADSas* ovules at stage 2-IV. Even if with a milder effect with respect to the *spl-1* case*, pSPL/NZZ::MADSas* fails in the differentiation of the MMC, that could be clearly identified in the wild type nucellus. (**F**) Bar plot showing the mean ± SEM of the percentage of ovules developing the MMC in wild type, *spl-1, pSPL/NZZ::MADSas L1* (*shp1,2,STK/STK*), *pSPL/NZZ::MADSas L2* (*shp1,2,STK/STK*) and *pSPL/NZZ::MADSas L3* (*shp1,2,stk*). The analysis has been performed on 5, 5, 5, 9 and 4 different pistils, respectively, for the wild type (122 ovules observed in total), *spl-1* (110 ovules observed in total), *pSPL/NZZ::MADSas L1* (113 ovules observed in total), *pSPL/NZZ::MADSas L2* (208 ovules observed in total), *pSPL/NZZ::MADSas L3* (67 ovules observed in total). Letters above the bars indicate homogenous categories with $p \leq 0.05$ as determined by one-way ANOVA with post-hoc Tukey HSD test. Single measures are represented with dots in the bars. Abbreviations: nu= nucella; fu= funiculus; ii= inner integument; oi= outer integument; in= integument; MMC= megaspore mother cell. Scale bar = 20 µm

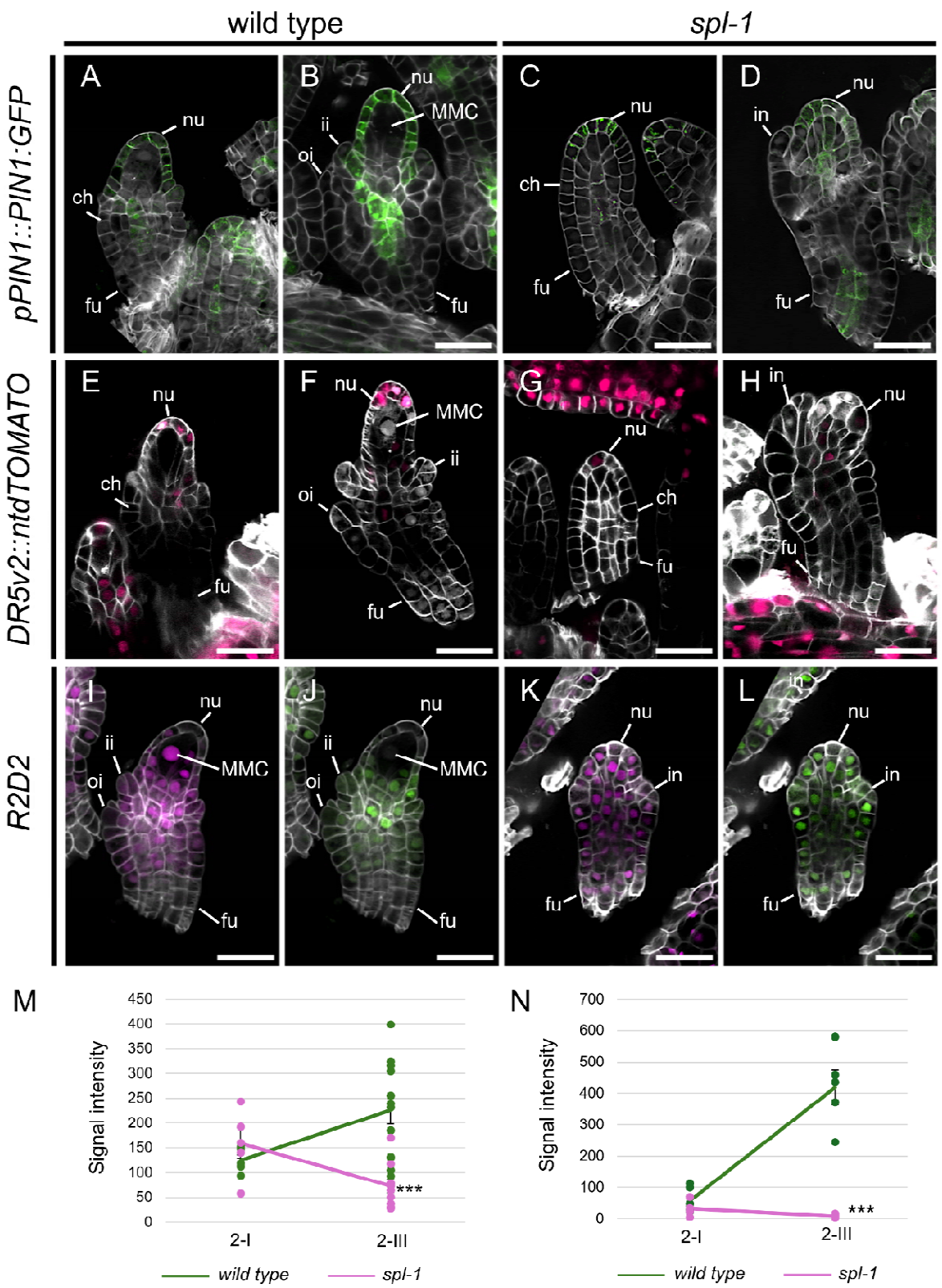

Figure 3: Auxin transport and signalling are impaired in the *spl-1* mutant ovule. (**A-D**) *pPIN1::PIN1:GFP* expression in wild type (**A**, **B**) and *spl-1* (**C**, **D**) ovules at stages 2-I

(**A, C**) and 2-III (**E**, **H**).*DR5v2* expression in wild type (**E**, **F**) and *spl-1* (**G**, **H**) ovules at stages 2-I (**E**, **G**) and 2-III (**F**, **H**). (**I**-**L**) *R2D2* reporter line in wild type (**I**, **J**) and *spl-1* (**K**, **L**) ovules at stage 2-III, showing mDII-tdTOMATO (**I**, **K**) and DII-VENUS (**J**, **L**) accumulation. (**I**-**L**) (**M**) Line graph showing the mean ± SEM of PIN1-GFP signal intensity in the L1 layer of wild type and *spl-1* ovules at stages 2-I and 2-III. Measurements have been performed on 5 wild type and 5 *spl-1* different ovules at stage 2-I and on 12 wild type and 10 *spl-1* different ovules at stage 2-III. Asterisks represent the statistical significance as determined by student's t-test, two-tailed distribution homoscedastic, confronting the mutant with the wild-type condition at each timepoint. *** = $p \leq 0.001$. Single measures are represented with dots in correspondence to the lines ends. (**N**) Line graph showing the mean ± SEM of the tdTOMATO signal intensity, from the *DR5v2* reporter, in the L1 layer of wild type and *spl-1* ovules at stages 2-I and 2-III. Measurements have been performed on 6 wild type and 4 *spl-1* different ovules at stage 2-I and on 5 wild type and 5 *spl-1* different ovules at stage 2-III. Asterisks represent the statistical significance as determined by student's t-test, two-tailed distribution homoscedastic, confronting the mutant with the wild-type condition at each timepoint. *** = $p \leq 0.001$. Single measures are represented with dots in correspondence to the lines ends. Abbreviations: nu= nucella; ch= chalaza; fu= funiculus; ii= inner integument; oi= outer integument; in= integument; MMC= megaspore mother cell. Scale Bars = 20 µm.

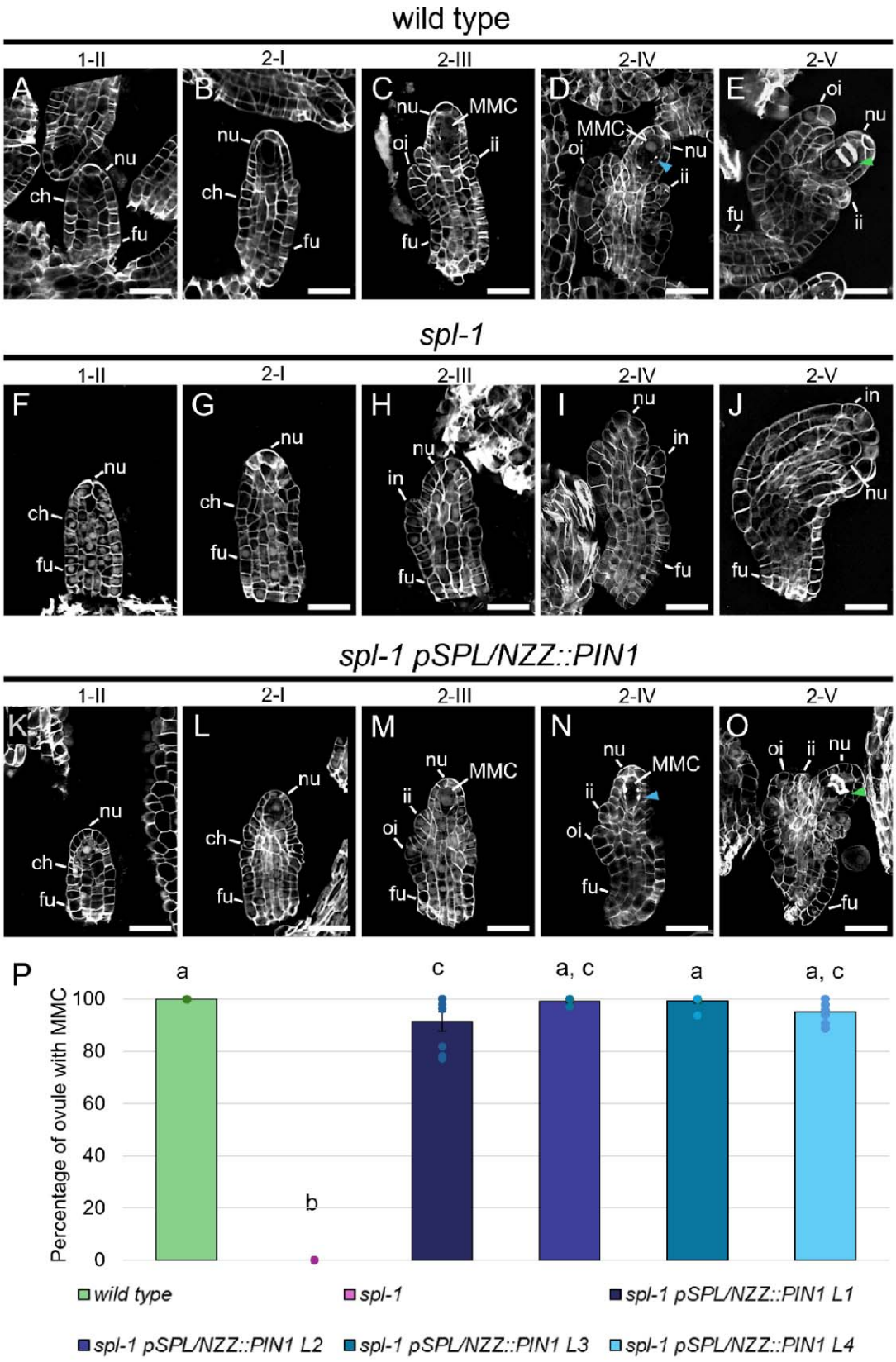

Figure 4: PIN1 expression derived by *SPL/NZZ* regulatory sequences is sufficient to restore the MMC differentiation in the *spl-1* ovule. (**A-E**) wild type ovules at stage 1-II

(**A**), 2-I (**B**), 2-III (**C**), 2-IV (**D**) and 2-V (**E**). At stage 2-III, the MMC is differentiated (**C**) while callose depositions can be observed at stage 2-IV (**D**). At stage 2-V (**E**), the MMC meiosis ends as denoted by the formation of the two meiotic plates. (**F**-**J**) *spl-1* ovules at stage 1-II (**F**), 2-I (**G**), 2-III (**H**), 2-IV (**I**) and 2-V (**J**). In the *spl-1* mutant the MMC do not differentiate (**H**, **I**). (**K**-**O**) *spl-1 pSPL/NZZ::PIN1* ovules at stage 1-II (**K**), 2-I (**L**), 2-III (**M**), 2-IV (**N**) and 2-V (**O**). Restoring *PIN1* expression in the *spl-1* nucellus is sufficient to drive the MMC differentiation (**M**, **N**). The MMC can be observed at stage 2-III (**M**). As in the wild-type situation (**D**) the MMC is surrounded by callose depositions at stage 2-IV (**N**) and correctly goes through the meiotic process (**O**). (**P**) Bar plot showing the mean ± SEM of the percentage of ovules developing the MMC, in wild type, *spl-1* and four *spl-1 pSPL/NZZ::PIN1* independent lines. The analysis has been performed on 8, 7, 8, 6, 8 and 9 different pistils, respectively, for the wild type (202 ovules observed in total), *spl-1* (238 ovules observed in total), *spl-1 pSPL/NZZ::PIN1 L1* (294 ovules observed in total), *spl-1 pSPL/NZZ::PIN1 L2* (196 ovules observed in total), *spl-1 pSPL/NZZ::PIN1 L3* (274 ovules observed in total) and *spl-1 pSPL/NZZ::PIN1 L4* (364 ovules observed in total). Letters above the bars indicate homogenous categories with $p \leq 0.05$ as determined by one-way ANOVA with post-hoc Tukey HSD test. Single measures are represented with dots in the bars. Abbreviations: nu= nucella; ch= chalaza; fu= funiculus; ii= inner integument; oi= outer integument; in= integument; MMC= megaspore mother cell. Blue arrowheads indicate the callose depositions. Green arrowhead indicates the meiotic plates. Scale bar = 20 µm

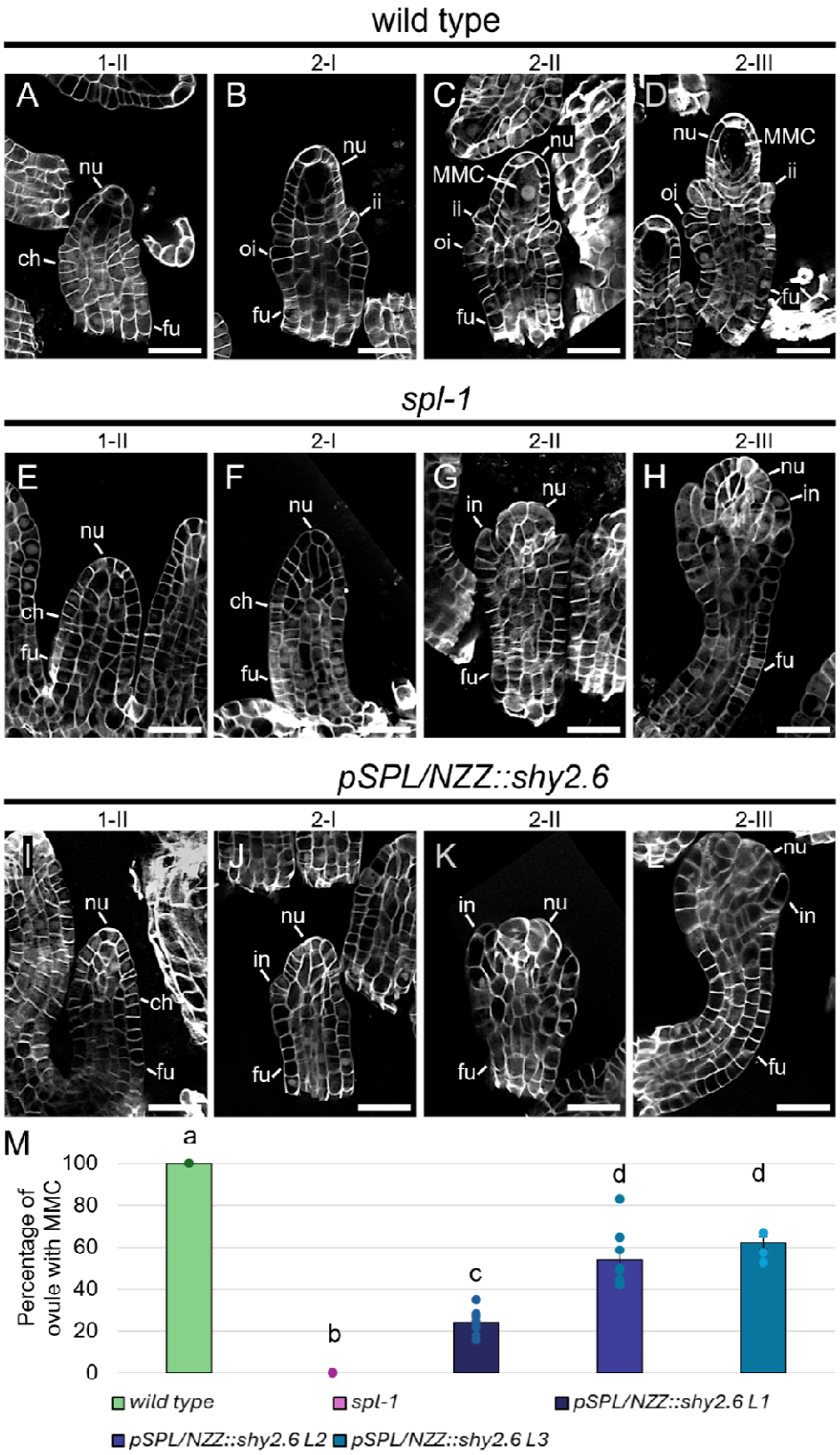

Figure 5: *shy2.6* expression in the nucellus impair the MMC differentiation. (**A-D**) wild type ovules at stage 1-II (**A**), 2-I (**B**), 2-II (**C**) and 2-III (**D**). (**E-H**) *spl-1* ovules at stage 1-II

(**E**), 2-I (**F**), 2-II (**G**) and 2-III (**H**). (**I**-**L**) *pSPL/NZZ:shy2.6* ovules at stage 1-II (**I**), 2-I (**J**), 2-II (**K**) and 2-III (**L**). *shy2.6* expression in the wild-type nucellus impair the MMC differentiation, mimicking the *spl-1* phenotype (**G**, **H, K**, **L**). (**M**) Bar plot showing the mean ± SEM of the percentage of ovules showing an MMC in wild type, *spl-1* and *pSPL/NZZ::shy2.6* lines. The analysis has been performed on 3, 4, 8, 9 and 5 different pistils, respectively, for the wild type (113 ovules observed in total), *spl-1* (157 ovules observed in total), *pSPL/NZZ::shy2.6 L1* (356 ovules observed in total), *pSPL/NZZ::shy2.6 L2* (378 ovules observed in total) and *spl-1 pSPL/NZZ::shy2.6* L3 (202 ovules observed in total). Letters above the bars indicate homogenous categories with $p \leq 0.05$, as determined by one-way ANOVA with post-hoc Tukey HSD test. Single measures are represented with dots in the bars. Abbreviations: nu= nucella; ch= chalaza; fu= funiculus; ii= inner integument; oi= outer integument; in= integument; MMC= megaspore mother cell. Scale bars = 20µm.

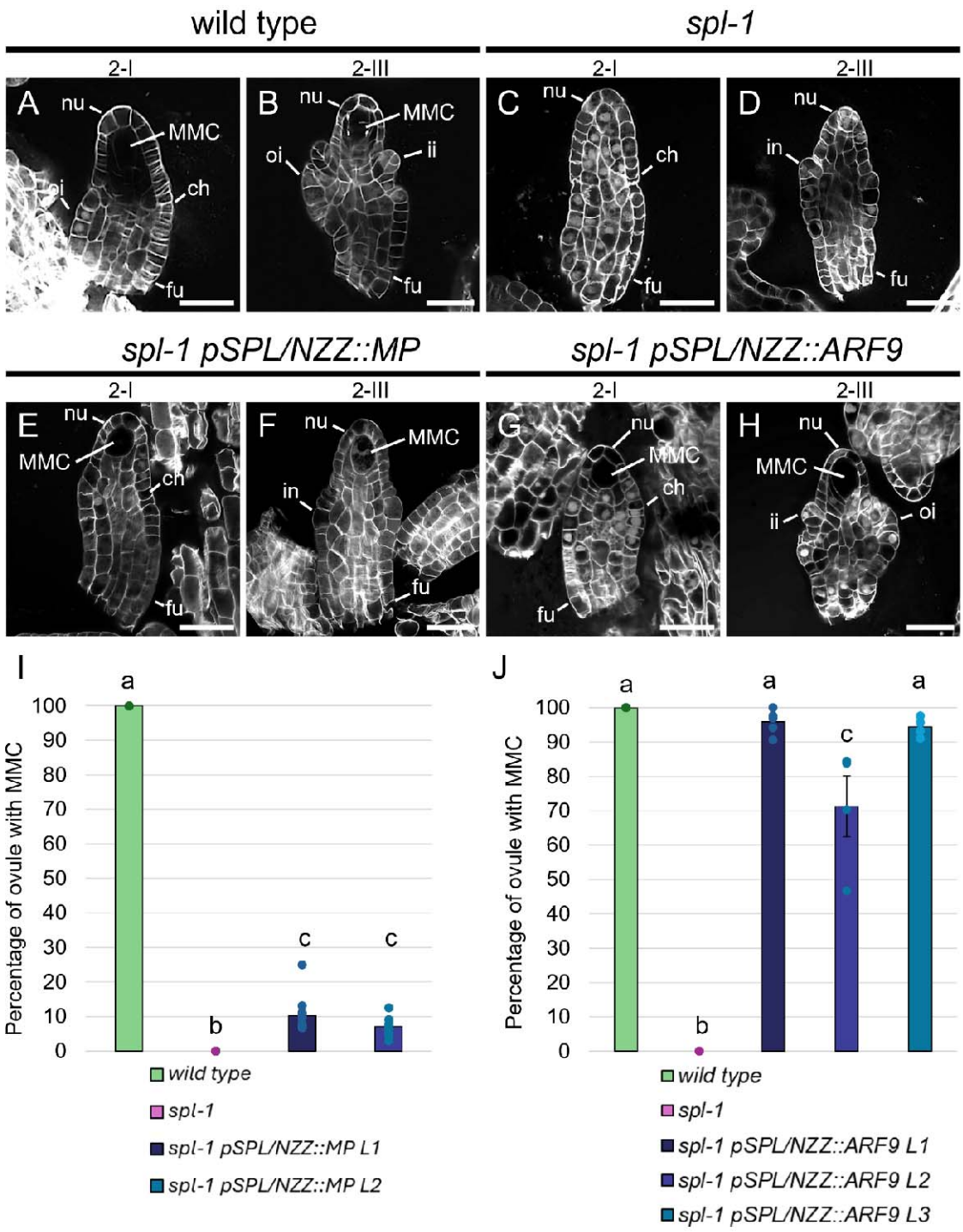

Figure 6: Increase ARF levels in the *spl-1* nucellus partially restore the MMC differentiation. (**A, B**) wild type ovules at stage 2-I (**A**) and 2-III (**B**). (**C, D**) *spl-1* ovules at stage 2-I (**C**) and 2-III (**D**). (**E**, **F**) *spl-1 pSPL/NZZ::MP* ovules at stage 2-I (**E**) and 2-III (**F**). (**G**, **H**) *spl-1 pSPL/NZZ::ARF9* ovules at stage 2-I (**G**) and 2-III (**H**). While increasing *MP* expression only partially restores the MMC differentiation, *pSPL/NZZ::ARF9* rescues the

MMC differentiation in *spl-1* (**I**) Bar plot showing the mean ± SEM of the percentage of ovules showing an MMC in wild type, *spl-1* and *spl-1 pSPL/NZZ::MP* lines. The analysis has been performed on 5, 8, 12 and 9 different pistils for the wild type (150 ovules observed in total), *spl-1* (304 ovules observed in total), *spl-1 pSPL/NZZ::MP L1* (362 ovules observed in total) and *spl-1 pSPL/NZZ::MP L2* (270 ovules observed in total). Letters above the bars indicate homogenous categories with $p < 0.05$, as determined by one-way ANOVA with post-hoc Tukey HSD test. Single measures are represented with dots in the bars. (**J**) Bar plot showing the mean ± SEM of the percentage of ovules showing an MMC in wild type, *spl-1* and *spl-1 pSPL/NZZ::ARF9* lines. The analysis has been performed on 4, 4, 5, 4, 4 different pistils for the wild type (157 ovules observed in total), *spl-1* (131 ovules observed in total), *spl-1 pSPL/NZZ::ARF9 L1* (193 ovules observed in total), *spl-1 pSPL/NZZ::ARF9 L2* (115 ovules observed in total) and *spl-1 pSPL/NZZ::ARF9 L3* (177 ovules observed in total). Letters above the bars indicate homogenous categories with $p \leq 0.05$, as determined by one-way ANOVA with post-hoc Tukey HSD test. Single measures are represented with dots in the bars. Abbreviations: nu= nucella; ch= chalaza; fu= funiculus; ii= inner integument; oi= outer integument; in= integument; MMC= megaspore mother cell. Scale bars = 20µm.

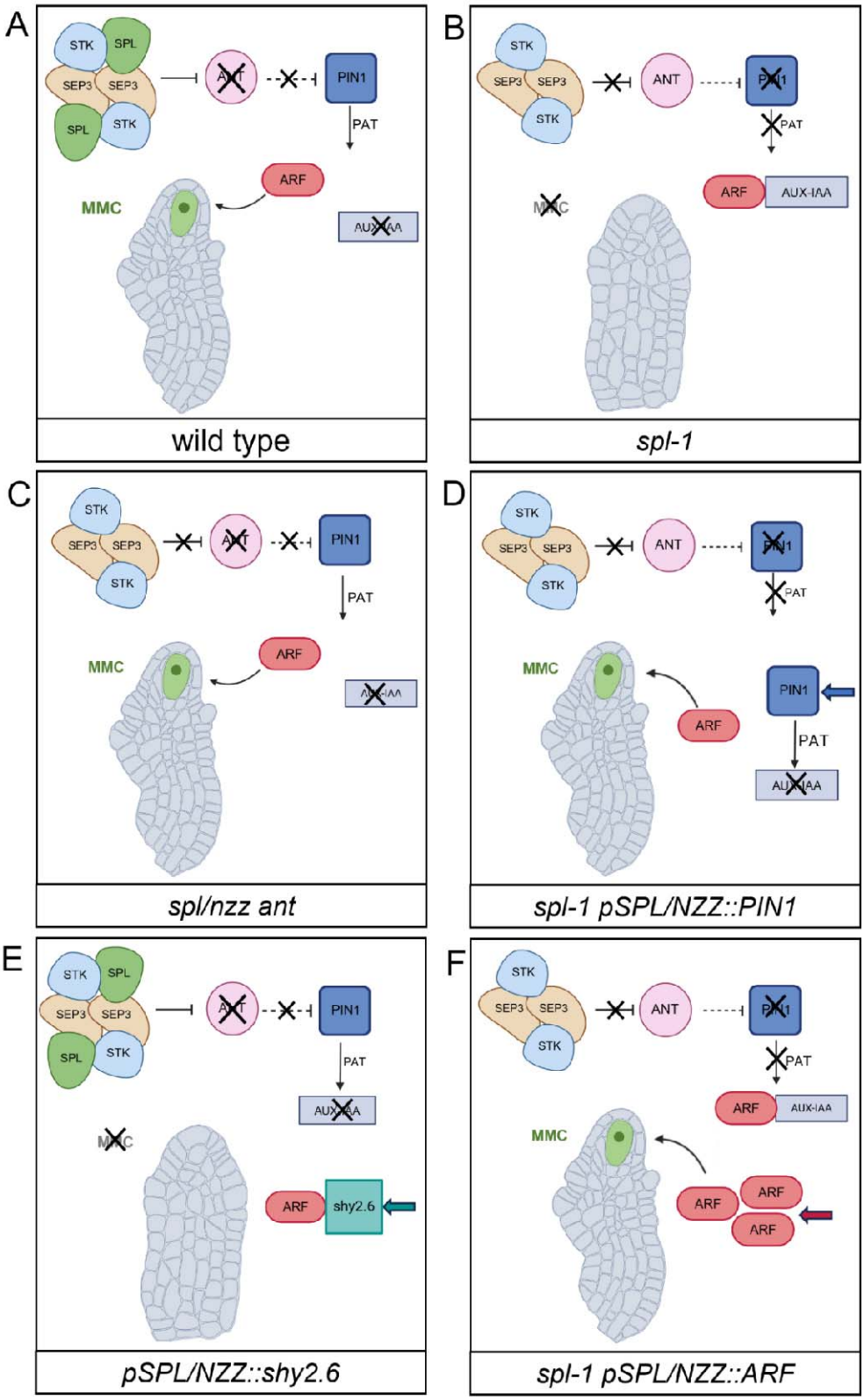

Figure 7: SPL/NZZ, by indirectly regulating *PIN1* expression, determine the MMC differentiation though an auxin-dependent network. (**A**) In the wild type, SPL/NZZ interacts with the ovule-identity MADS-domain complex to inhibit *ANT* expression,

facilitating auxin accumulation in the nucellus and subsequently enabling the ARF-mediated auxin response required to promote the MMC specification. (**B**) In the *spl/nzz* mutant, *ANT* is expressed in the nucellus, leading to the downregulation of *PIN1* and to an auxin subthreshold concentration, which disable the post-translational activation of the ARFs, necessary for MMC formation**.** (**C**) In the *ant spl/nzz* mutant, the inhibition of *PIN1* does not take place, allowing the formation of the MMC even in the absence of SPL/NZZ. (**D**) Expressing *PIN1* under the control of the *SPL/NZZ* promoter in the *spl/nzz* mutant, is sufficient to restore the proper auxin threshold in the nucellus and the ARF-mediated auxin response required for the MMC specification. (**E**) The expression of the non-degradable *shy2.6* isoform in the wild-type nucellus leads to the post-translational deactivation of the ARFs, resulting in the absence of the MMC formation. (**F**) Increase ARF levels in the *spl/nzz* mutant can overcome the repressive state caused by Aux/IAAs over-accumulation, determining the MMC differentiation.